LUND UNIVERSITY

FEM MODELLING OF PILED RAFT FOUNDATIONS IN TWO AND THREE DIMENSIONS

ANDRÉ RYLTENIUS

Geotechnical Engineering

Master's Dissertation

Department of Construction Sciences
Geotechnical Engineering

ISRN LUTVDG/TVGT--11/5046--SE (1-73)
ISSN 0281-6679

FEM MODELLING OF PILED RAFT FOUNDATIONS IN TWO AND THREE DIMENSIONS

Master's Dissertation by

ANDRÉ RYLTENIUS

Supervisors:

Ola Dahlblom, *Professor,*
Dept. of Construction Sciences, LTH, Lund

Lars Johansson, *Lic.,*
Ramböll Sverige AB

Examiner:

Per Johan Gustafsson, *Professor*
Dept. of Construction Sciences, LTH, Lund

Printed by Media-Tryck LU, Lund, Sweden, September 2011 *(Pl)*.

For information, address:
Geotechnical Engineering, LTH, Lund University, Box 118, SE-221 00 Lund, Sweden.
Homepage: http://www.byggvetenskaper.lth.se/geoteknik

Abstract

In conventional design of pile foundations, all loads are taken by the piles, i.e. the contact pressure between the raft and the soil is neglected. In the last decades geotechnical engineers have started to take this pressure into account in design of pile foundation. Such a foundation, where the raft and the piles interact to transfer the loads to the ground, is in this dissertation called piled raft foundation or piled raft.

Analysis of piled rafts requires numerical methods, due to complex soil-structure interaction. In this dissertation four different modelling approaches for analysis of piled raft foundation are compared; a full three dimensional finite element method model (FEM model) and also three plane strain FEM models (i.e. two dimensional models). All models are carried out by using programs developed by Plaxis, i.e. Plaxis 3DFoundation and Plaxis 2D, respectively. The plane strain models are similar but differ in the way of modelling the interaction between the piles and the soil. The first plane strain model is introduced in Chapter 3.4.2. Since this model produce questionable results, due to too weak modelling of the pile-soil interaction, two alternative models are introduced in Chapter 8.4 and 8.5 (called AM1 and AM2).

Piled raft foundations are three dimensional problems, in a two dimensional analysis one has to introduce simplifications and thereby inaccuracies. However, it could still be convenient to use this method since it is faster and the software is less expensive. The inaccuracies in a 2D model compared to a 3D model will vary depending on the characteristics of the problem. The object of the work is to study the inaccuracies and how these changes as the characteristics of the problem change.

The work starts with a study of previous master dissertations and other literature. To get a better understanding of Plaxis, a sheet pile wall is then modelled in Plaxis 2D. Subsequently, a hypothetical piled raft is analysed in Plaxis 2D and 3DFoundation to illustrate the different modelling approaches. The piled raft is square with the piles distributed uniformly, and it is loaded vertically and uniformly. Finally, a parametric study of the different models is performed, where two parameters for the hypothetical piled raft are varied, i.e. pile spacing and the shape of the piled raft (rectangular, with different base to length relations).

When comparing the results, the 3D model is considered “true” and the maximum values are examined. In general for the piled rafts analysed, the two dimensional models (AM1 and AM2) overestimate the settlement (~30%), the raft bending moment (~30%) and the pile force (~10%). As the pile spacing decreases, the pile force from the 2D models resembles the 3D models more. While the settlement and the bending moment coincides less as the pile spacing decreases. As the length of the piled raft increases, the settlements and pile force from the 2D model converge towards the 3D results, which is expected since the problem get more two dimensional. However, a problem occurs as the raft gets non quadratic. The maximal differential settlement will then take place in the longer direction, and to calculate it, calculations have to be made for sections in the longer direction, were the plane strain condition is less satisfactory. This problem is off course less significant when the differential settlements are small as for a piled raft with a very stiff raft.

The inaccuracies occurring in the alternative plane strain models are more or less significant in all cases and the 2D models should be used carefully. Especially when calculating differential settlements or the bending moment in the longer direction. The plane strain models generate similar settlement and pile force as a 3D model when pile spacing is narrow and the piled raft shape is greater than 1:2, i.e. when the problem is more two dimensional. However, the piled rafts analysed are simple and as the problems get more complex the conclusions drawn here could be questionable, and the choice of model should lean towards a 3D model.

Sammanfattning

Pålgrundläggning dimensioneras traditionellt så att all last tas av pålarna. Man bortser därmed från den last som kan överföras mellan plattan och jorden via kontakttryck. Allt mer börjar geotekniker ta hänsyn till detta kontakttryck, och därmed utnyttjas grundläggningen mer optimalt. En pålgrundläggning där plattan och pålarna samverkar för att bära lasten kallas samverkansgrundläggning.

Dimensionering av samverkansgrundläggning kräver numeriska beräkningsmetoder, då samverkan mellan jord, platta och pålar blir komplex. I detta arbete studeras och jämförs fyra olika sätt att modellera samverkansgrundläggning med numeriska metoder; en fullskalig tre dimensionell finita element modell (FEM-model) och tre två dimensionella FEM-modeller, där de två dimensionella är plan töjningsmodeller. Samtliga modellerna kommer att modelleras med hjälp av program utvecklade av Plaxis, Plaxis 3DFoundation respektive Plaxis 2D. De olika 2D-modellerna är lika, men olika sätt att modellera amverkan mellan jord och påle har använts. Den första plan töjningsmodellen är introducerad i kapitel 3.4.2, då denna typ av modellering genererar orimliga svar (på grund av för vek modellering av samverkan mellan påle och jord), introduceras två alternativa beräkningsmodeller i kapitel 8.4 och 8.5 (vilka kallas AM1 och AM2).

Samverkansgrundläggning är ett tredimensionellt problem och i en tvådimensionell modell introduceras förenklingar och därmed avvikelser. Trots detta kan en tvådimensionell modell vara att föredra, då den är snabbare och dess programvara är billigare. Avvikelserna i en 2D modell har varierande storlek beroende på problemets utformning. Målet med detta arbete är att studera avvikelserna och hur de varierar då problemets utformning förändras.

Arbetet inleds med en litteraturstudie för att samla in information från liknande arbeten och facklitteratur. För att få en känsla för programvaran och även för jordmodeller och konstruktioners beteende i jord analyseras därefter en spont. Spontens deformationer vid urschaktningen har mätts och beräkningsresultatet kan därför jämföras mot mätvärden. Därefter modelleras en idealiserad samverkansgrundläggning i två och tre dimensioner, detta för att illustrera de två beräkningsmetoderna. Plattan är kvadratisk och pålarna är jämnt fördelade, konstruktionen är belastad med en vertikal och jämnt utbredd last. Slutligen utförs en parameterstudie för den idealiserade samverkansgrundläggningen där påltätheten och plattans längd-bredd förhållande varieras.

Studien visar att 2D-modellerna (AM1 och AM2) generellt överskattar sättningen (~30%), momentet i plattan (~30%) och pålkraften (~10%) jämfört med 3D-modellerna. Differentialsättningen och pålkraften från 2D-modellerna skiljer sig mindre från 3D-modellerna då påltätheten ökar, medan avvikelsen gällande sättning och momentet ökar. När plattan blir längre konvergerar sättningen och pålkraften från 2D-modellerna mot de från 3D-modellerna, vilket är förväntat då problemet blir mer två dimensionellt. När plattan blir längre uppstår dock ett problem, den maximala differentialsättningen uppstår i den långa ledden och för att beräkna denna krävs beräkningar för snitt i den långa ledden, där antagandet om plan töjning är sämre. Detta problem kommer dock att vara mindre signifikant för samverkansgrundläggningar med mycket styva plattor där differentialsättningen är liten.

I de flesta fall som har studerats är skillnaden mellan 2D-beräkningarna och 3D-beräkningarna signifikant. Speciellt för avlånga plattor när differentialsättning och böjmoment söks i den långa ledden. Plan töjningsmodellerna generera dock sättningar och pålkrafter som liknar de från 3D-beräkningarna, när pålavståndet är litet och plattan är avlång, alltså när problemet är mer tvådimensionellt. Samverkansgrundläggningarna i detta arbete är dock idealiserade och enkla och när problemen blir mer komplexa och tre dimensionella bör en 3D-model användas.

Preface

The study described in this master's dissertation is the final part of the Civil Engineering programme at the Faculty of Engineering, Lund University.

The work was carried out at Ramböll Sverige AB in Malmö, in cooperation with the Division of Structural Mechanics, Lund University.

I would like to thank my supervisors Lars Johansson, geotechnical engineer at the AMC (Analysis Modelling and Calculation) group at Ramböll, and Professor Ola Dahlblom at the Division of Structural Mechanics for their valuable support and help.

I would also want to thank the Department of Building Design at Ramböll for providing me with an office place and a fun time during my work.

André Ryltenius
Malmö, February 2011

Table of contents

1. Introduction

1.1. Background

When founding a building the simplest structure considered is a raft, which is suitable in areas with good soil. Piled foundation is an old method to improve the load capacity and reduce the settlements for a raft foundation in areas with insufficient soil. The main purpose of this method is to transfer the load via the piles to firm rock or stiffer soil, i.e. further down in the ground.

In conventional design of piled foundation, all loads are designed to be transferred via the piles to the soil. Hence, neglecting the pressure, which could be, transferred from the raft directly to the soil by contact pressure. In the last decades geotechnical engineers have started to design piled foundation more optimised by allowing a part of the pressure to transfer directly from the raft to the ground. Such a foundation, where the raft and the piles interact to transfer the loads to the ground is called piled raft foundation or piled raft.

Piled raft foundations have a complex soil-structure interaction. In analysis care must be taken to pile-soil interaction, pile-pile interaction, raft-soil interaction, and pile-raft interaction. This often requires numerical methods. In this dissertation four different methods for analysis of piled raft foundation are compared; a full three dimensional finite element method model (FEM model) and three plane strain (2D) FEM models, all by using programs developed by Plaxis, i.e. 3DFoundation and Plaxis 2D, respectively. The plane strain models are similar but use different approaches to model the interaction between the piles and the soil.

Piled raft foundations are three dimensional problems, in a two dimensional analysis one has to introduce simplifications and thereby inaccuracies. However, it could still be convenient to use this method since it is faster and the software is less expensive.

1.2. Objective

The object is to compare FEM analysis of piled raft foundations in two and three dimensions, using Plaxis 2D and 3DFoundation, respectively.

1.3. Disposition

The work starts with a study of previous master dissertations and literature divided into; Sheet pile wall, Chapter 2, Piled raft foundation, Chapter 3 and Plaxis, Chapter 4.

To get a better understanding of Plaxis, a sheet pile wall is analysed in Plaxis 2D and the result is compared with measured displacements, presented in Chapter 5.

In Chapter 6, a hypothetical piled raft foundation is analysed in Plaxis 2D to illustrate the two dimensional analysis method. A full three dimensional analysis is then carried out in Chapter 7 using Plaxis 3DFoundation, to illustrate the three dimensional method.

Finally in Chapter 8, a parametric study of the two analysis methods is performed. With focus on how the two models differ for varying geometries.

2. Sheet pile wall

2.1. Introduction

A sheet pile wall is a type of retaining wall. Retaining walls are installed, mainly, when a difference in ground elevation with a greater angle than the soil's angle of repose is wanted. Where the angle of repose is the maximum angle a soil can withstand without sliding. When the soil is forced into this state the soil wants to transform back to its natural state and lateral pressure towards the wall occurs, called lateral earth pressure. The main purpose of the wall is to resist this pressure. A typical retaining wall is illustrated in Figure 2.1.

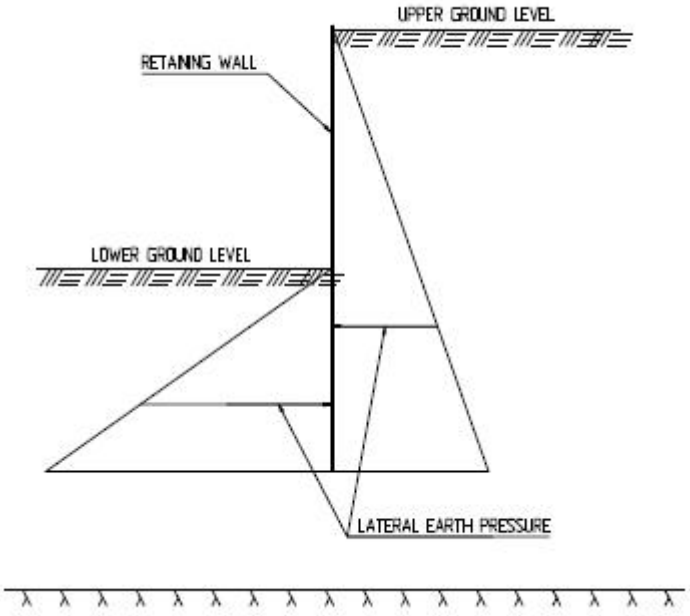

Figure 2.1. Typical retaining wall.

The sheet pile wall consists of steel plates which are driven into the ground, the plate's cross section is shown in Figure 2.2. The wall is often reinforced in the upper parts, either by a tieback or a strut to ensure rotational stability. Another alternative is to mount the wall to firm rock. The sheet pile wall is often used when constructing temporary support of excavation walls, as in the sheet pile wall analysed in this work.

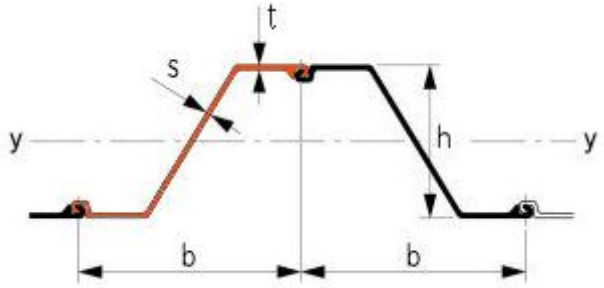

Figure 2.2. Cross section of two sheet piles interlocked [13].

This chapter will describe the sheet pile wall's function, which is important to understand prior to the analysis of the sheet pile wall in Chapter 5.

2.2. Stress, strain and strength in soil

Before lateral earth pressure acting on the wall is brought up, a short introduction of stress and strain in soil and also strength of soil is presented. These are components closely related to the important lateral earth pressure.

2.2.1. Assumptions

Soil is a natural material that consists of three phases, i.e. particles, water and air. These three phases vary within the material and the mechanics of soil is therefore complex. Because of the complexity of soil, one needs to introduce simplifications and assumptions when modelling the mechanical behaviour of soil. When talking about stress and strain in basic soil mechanics, one often makes the following assumptions about soil; it is a continuous, homogeneous, isotropic and linear elastic material [1]. These assumptions are also present in the following presentation.

2.2.2. Stress and strain

The coordinate system when conducting stress and strain analysis is normally, in geotechnical matters, defined with the x- and y-directions horizontally and the z-direction vertically. The stress state in soil is expressed by six stress and six strain components along the coordinate axes, i.e. three normal stress components σ_x, σ_y and σ_z with three corresponding normal strains $\varepsilon_x, \varepsilon_y$ and ε_z, and three shear-stress components, τ_{xy}, τ_{xz} and τ_{yz} with corresponding shear strains γ_{xy}, γ_{xz} and γ_{yz}. Further on, compressive stress and strain is normally defined as positive and tensile stress as negative, since tension is rare in soil.

The stress state described until now is general and defined in three dimensions. However, retaining walls are a fairly two dimensional problem and are often analysed in two dimensions. The stress state is then expressed as in Figure 2.3.

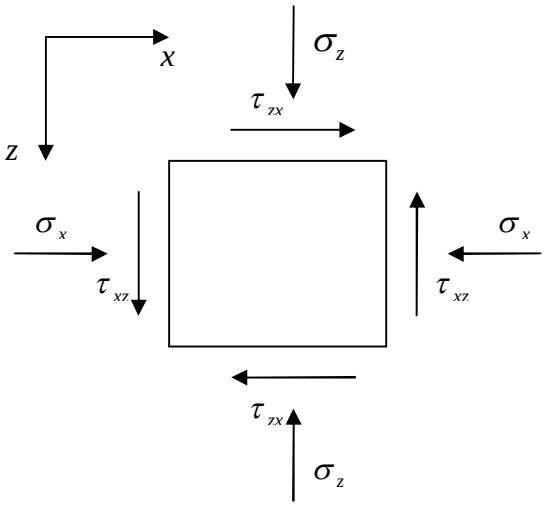

Figure 2.3. Two dimensional stress state.

Soil distributes stress by two of its three phases, i.e. the solid particles and the pore water. The sum of these two is called total stress. The stress transferred by the solid particles is called effective stress and is an important stress component in soil mechanics, since failure in soil is

coupled to this stress. Failure in soil is explained in the following chapter. Effective stress is expressed as

$$\sigma' = \sigma - u \qquad (2.1)$$

where σ is the total stress and u is the pore pressure.

Most loads causing stress in soil are vertical. This could be both body stress and induced stress, i.e. stress occurring due to the deadweight of the soil and stress occurring due to external loads, respectively. Horizontal stress does however exist but is indirectly caused by vertical stresses. Lateral earth pressure occurs due to horizontal stress and it is therefore important when designing retaining walls. The ratio between vertical stress and horizontal stress is called coefficient of lateral earth pressure, defined as

$$K = \frac{\sigma'_x}{\sigma'_z} \qquad (2.2)$$

The loads and the vertical stresses are often known, one can thereby use this factor to calculate the horizontal stress. K normally varies between 0.3 and 3 [1]. How the K-factor is conducted is discussed in chapter 2.3.

As already mentioned in the assumptions, soil is modelled as a liner-elastic material, i.e. having a stress-strain relation that is linear elastic. Hence, obeying Hooke's law

$$\sigma = E\varepsilon \qquad (2.3)$$

Later in this dissertation, when presenting Plaxis, the relation between stress and strain is studied more thorough and different relations are presented. This relation is important when modelling soil, but is kept simple in this chapter to maintain the object of this chapter, i.e. to describe a sheet pile wall's function.

2.2.4. Mohr's-circle and principal stress

Mohr's-circle is a representation of the two dimensional stress in soil. The stresses earlier shown in Figure 2.2 are plotted in the $\sigma\tau$-plane, for all angles of the element. A typical Mohr's-circle is illustrated in Figure 2.4.

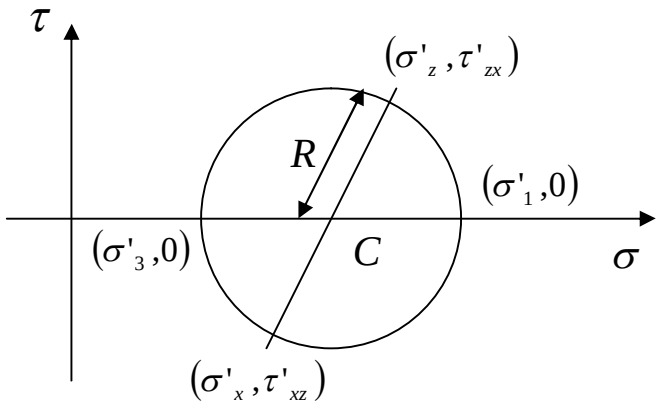

Figure 2.4. Mohr's-circle.

For a certain angle all shear stresses in the element are zero. The normal stresses acting on this element are called the principal stresses, defined as σ_1 and σ_3 in the figure. σ_1 is called the major principal stress and σ_3 the minor. These are the largest and the smallest normal stress, respectively, occurring in the soil element. The magnitude of σ_1 and σ_3 could be derived using basic trigonometry and is [1][2]

$$\sigma_1 = C + R = \frac{\sigma_x + \sigma_z}{2} + \sqrt{\left[\frac{\sigma_x - \sigma_z}{2}\right]^2 + \tau_{zx}^2} \qquad (2.4a)$$

$$\sigma_3 = C - R = \frac{\sigma_x + \sigma_z}{2} - \sqrt{\left[\frac{\sigma_x - \sigma_z}{2}\right]^2 + \tau_{zx}^2} \qquad (2.4b)$$

where C is the centre of the circle and R is the radius of the circle.

2.2.5. Mohr-Coulomb's failure criterion and strength

Strength is the maximum stress a soil can withstand without failing. Failure in soil is, in general, caused by shear stress, i.e. shear failure [1]. Shear failure occurs when particles slide or roll past each other [1]. Failure due to compression would be particles crushing, but, since the particles start sliding and rolling, when exposed to compression, they fail in shear and not compression [1].

Shear strength, i.e. ability to resist sliding and rolling, depends on the interaction between the particles. This interaction is both due to friction and cohesion. Where friction is mechanical resistance and cohesion is primarily chemical resistance. The shear strength due to friction was found and expressed by the French physicist C. A. Coulomb 1773 as [2]

$$\tau_s = \sigma' \tan(\phi') \qquad (2.5a)$$

where σ' is the effective stress acting on the shear surface and ϕ' is the friction angle.

This expression is called Coulomb's law of friction. One could note that the effective parameters are used, which is due to the non-existing shear strength of water. Hence, the shear-strength is only affected by the effective part of the stress.

To account for the cohesion, a modified version of the Coulomb's shear strength is used [2]

$$\tau_s = c + \sigma' \tan(\phi') \qquad (2.5b)$$

where c is the cohesive strength.

Coulomb's law of friction could be placed together with Mohr's-circle in the $\sigma\tau$ -plane, as in Figure 2.5.

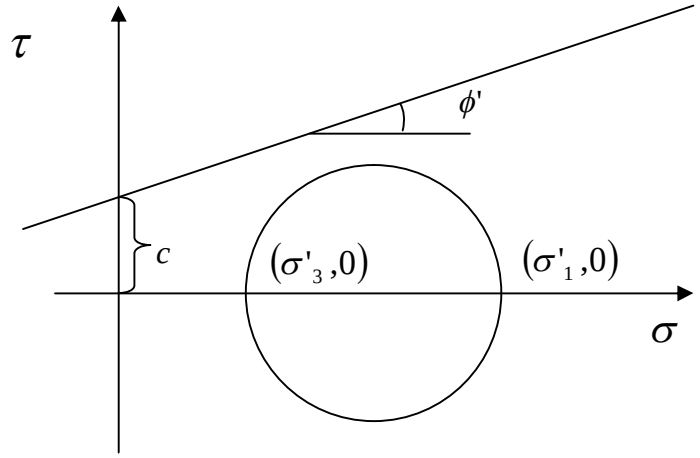

Figure 2.5. Coulomb law of friction and Mohr's-circle.

According to Mohr-Coulomb's failure criterion failure occurs at the stress state represented by a Mohr's-circle touching the line formed by Coulomb's law of friction, see Figure 2.6.

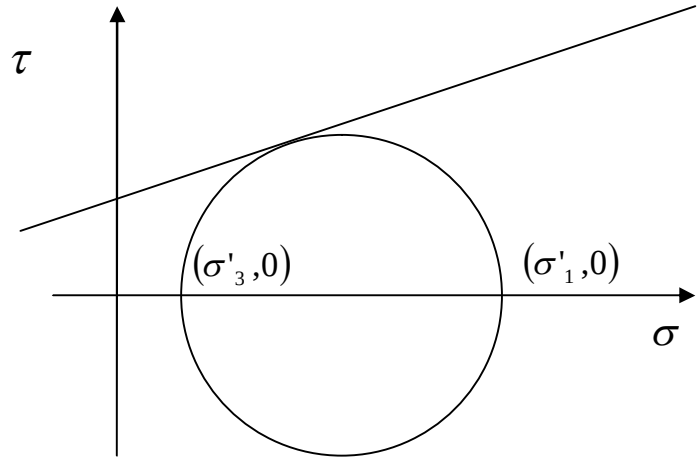

Figure 2.6. Mohr-coulomb failure criterion.

The principal stresses at failure could be derived from the figure of Mohr-Coulomb's failure criterion with basic trigonometry and are for a frictional soil [2]

$$\sigma'_1 = \sigma'_3 \frac{1+\sin(\phi')}{1-\sin(\phi')} \qquad (2.6a)$$

and for a frictional-cohesive soil

$$\sigma'_1 = \sigma'_3 \frac{1+\sin(\phi')}{1-\sin(\phi')} + 2c' \frac{\cos(\phi')}{1-\sin(\phi')} \qquad (2.6b)$$

These two expressions could be simplified to [2]

$$\sigma'_1 = \sigma'_3 \tan^2\left(45+\frac{\phi'}{2}\right) \qquad (2.7a)$$

and

$$\sigma'_1 = \sigma'_3 \tan^2\left(45+\frac{\phi'}{2}\right) + 2c' \tan\left(45+\frac{\phi'}{2}\right) \qquad (2.7b)$$

Further on, the centre and the radius, of the Mohr's-circle, at failure for a frictional soil is [2]

$$C = \frac{\sigma'_1}{1+\sin(\phi')} \qquad (2.8a)$$

$$R = \sigma'_1 \frac{\sin(\phi')}{1+\sin(\phi')} \qquad (2.8b)$$

and for a frictional-cohesive soil

$$C = \sigma'_1 \frac{1}{1+\sin(\phi')} - c\tan\left(45-\frac{\phi'}{2}\right) \qquad (2.9a)$$

$$R = \sigma'_1 \frac{\sin(\phi')}{1+\sin(\phi')} + c\tan\left(45-\frac{\phi'}{2}\right) \qquad (2.9b)$$

2.3. Horizontal stress

As earlier mentioned horizontal stress is important for retaining walls because it is a component of the lateral earth pressure. Three states are used to describe the condition of a soil's condition concerning horizontal stress; at-rest condition, active condition and passive condition [1]. When conducting these conditions, the wall is assumed to be rigid.

2.3.1. At-rest condition

The at-rest condition is, as the name indicates, the horizontal stress when a soil is at rest. In our case that would be the sheet pile wall being still. That is rarely the case since very small movements are adequate to out rule the at-rest condition [1]. However, basement walls are examples where this condition exists, due to its high stiffness. No movement in the soil implies no sliding in the soil thus no failure in the soil. The at-rest condition could therefore be illustrated by a Mohr's-circle not touching the Coulomb line, as in Figure 2.5.

2.3.2. Active condition

Let us assume a still sheet pile wall, retaining an excavation. The soil behind the wall is in at-rest conditions thus having a stress state as in Figure 2.5. If the wall now moves towards the excavation a small distance, the horizontal stress will diminish and thus expanding the Mohr's-Circle to the left (the vertical stress is constant). If this continues the Mohr's-circle will expand until failure.

A soil exhibiting this process is said to be in the active condition [1]. And the corresponding earth pressure is called active earth pressure. The vertical stress, which partly consists of the dead weight of the soil, is the major stress in this condition. The soil is therefore said to actively contribute to the earth pressure, thereby called active.

Since, the major principal stress in this condition is the vertical stress and the minor principal stress is the horizontal stress, one could express the active earth pressure with Equation 2.7a-b, for a soil without cohesion as

$$\sigma'_x = \sigma'_z \tan^2\left(45 - \frac{\phi'}{2}\right) \qquad (2.10a)$$

and with cohesion as

$$\sigma'_x = \sigma'_z \tan^2\left(45 - \frac{\phi}{2}'\right) - 2c'\tan\left(45 - \frac{\phi'}{2}\right) \qquad (2.10b)$$

where $\sigma'_1 = \sigma'_z$ and $\sigma'_3 = \sigma'_x$, according to the active condition.

The coefficient of active earth pressure for a soil without cohesion is then

$$K_A = \tan^2\left(45 - \frac{\phi'}{2}\right) \qquad (2.11a)$$

When expressing lateral earth pressure in cohesive soil an additional coefficient is introduced [2]

$$K_{AC} = 2\tan\left(45 - \frac{\phi'}{2}\right) \qquad (2.11b)$$

Yielding the following expression

$$\sigma'_x = \sigma'_z K_A - c' K_{AC} \qquad (2.12)$$

2.3.3. Passive condition

Once again, let us assume a still sheet pile wall, retaining an excavation. The soil surrounding the sheet pile is at rest. If we now consider the soil in front of the wall, below the excavation, and once again move the wall towards the excavation a small distance. The horizontal stress, in this area, will increase due to lateral compression, thereby first decreasing the Mohr's-circle until the same magnitude as the vertical stress is reached then expanding the Mohr's-circle to the right. If this continues the Mohr's-circle will expand until failure.

A soil exhibiting this process is said to be in the passive condition [1]. And the corresponding earth pressure is called passive earth pressure. The dead weight of the soil is in this scenario the minor stress and does not actively contribute to the earth pressure. It is therefore called passive earth pressure and passive condition.

The stress level is always higher in the passive condition, which is easily realized by reflecting on the definitions. This is important for obtaining equilibrium of the structure and is discussed further in the next chapter.

Since, the major principal stress in this condition is the horizontal stress and the minor principal stress is the vertical stress, one could express the passive earth pressure with equation 2.7a-b, for material without cohesion as

$$\sigma'_x = \sigma'_z \tan^2\left(45 + \frac{\phi'}{2}\right) \qquad (2.13a)$$

and with cohesion as

$$\sigma'_x = \sigma'_z \tan^2\left(45 + \frac{\phi}{2}'\right) + 2c'\tan\left(45 + \frac{\phi'}{2}\right) \qquad (2.13b)$$

Where $\sigma'_1 = \sigma'_x$ and $\sigma'_3 = \sigma'_z$, according to the passive condition. The coefficient of passive earth pressure for a soil without cohesion is then

$$K_P = \tan^2\left(45 + \frac{\phi'}{2}\right) \qquad (2.14a)$$

When expressing passive earth pressure in cohesive soil an additional coefficient is introduced [2]

$$K_{PC} = 2\tan\left(45 + \frac{\phi'}{2}\right) \qquad (2.14b)$$

Creating the following expression:

$$\sigma'_x = \sigma'_z K_P + c' K_{PC} \qquad (2.15)$$

2.4. Lateral earth pressure

The lateral earth pressure consists of the horizontal stress, derived earlier, and also, if present, the water pressure. The active earth pressure becomes

$$p_A = \sigma'_x + u = \sigma'_z K_A + u \qquad (2.16a)$$

$$p_{AC} = \sigma'_x + u = \sigma'_z K_A - c' K_{AC} + u \qquad (2.16b)$$

and the passive earth pressure

$$p_P = \sigma'_x + u = \sigma'_z K_P + u \qquad (2.17a)$$

$$p_{PC} = \sigma'_x + u = \sigma'_z K_P + c' K_{PC} + u \qquad (2.17b)$$

where the vertical stress consists of body stress and induced stress, as earlier mentioned. Both vary with depth, the body stress increases due to increased weight and the induced stress decreases due to load spread. Body stress varies linear with depth with the rate of the unit weight of the soil. There are some different models to describe the variation of induced stress, as the Boussineq's method, the Westergaard's method and the 2:1 method. A principle sketch of the lateral earth pressures acting on a sheet pile wall is illustrated below.

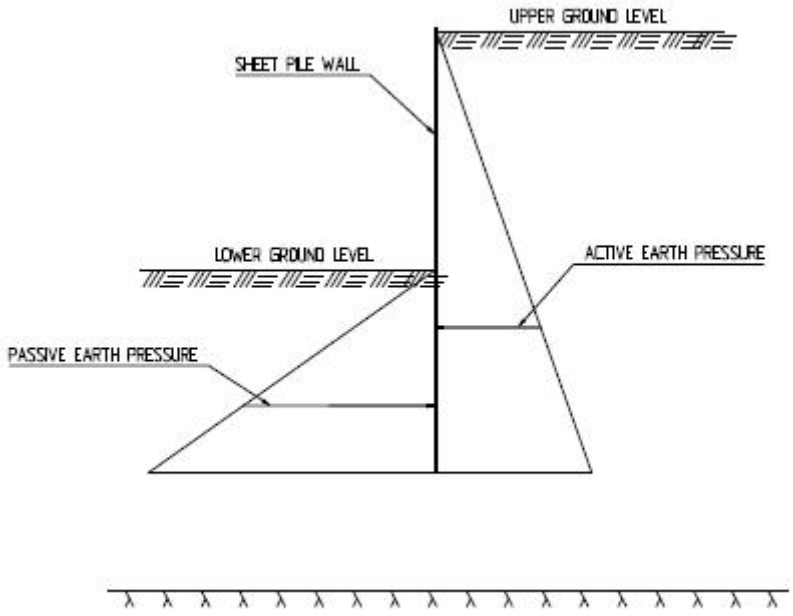

Figure 2.6. Typical sheet pile wall.

Failure will occur if the structure is not in equilibrium. An engineer must therefore ensure equilibrium horizontally and vertically, and moment equilibrium. One often starts by calculating the driving depth of the wall by assuming horizontal equilibrium. Horizontal and moment equilibrium is often ensured by applying tiebacks or struts in the upper parts of the wall. Vertical equilibrium is only an issue if these are applied diagonal, thus adding a vertical force. This force is taken by either driving the wall to the firm rock or by frictional forces that arise between the wall and the soil. An alternative to struts and anchors is to mount the wall to the firm rock.

There are some additional geotechnical issues when designing retaining walls, such as stability of the slope, stability of the excavation bottom and structural failure, but these are not presented further in this dissertation.

3. Piled raft foundation

3.1. Introduction

This chapter presents the general concept of piled raft foundation which is important to understand prior to the analysis of piled rafts in Chapter 6-8. First, raft foundation used without piles, raft-soil interaction, is presented. Then the piles stand alone and their interaction with the adjacent soil, i.e. pile-soil interaction, and also the pile-pile interaction when piles are placed in a group are discussed. In this dissertation focus is on piled raft foundation in soft clay which is the most common practice. The presentation of piles is therefore confined to cohesion piles, i.e. shaft bearing piles in cohesive soil (e.g. clay). Subsequently, methods for analysis of the pile-raft interaction are discussed.

3.2. Raft alone

3.2.1. Bearing capacity

The bearing capacity of a raft is the minor of the structural capacity and the geotechnical capacity. This dissertation focuses on the geotechnical capacity, which for a raft alone could be determined by using the general bearing capacity equation [3]

$$q_b = cN_c + qN_q + 0.5\gamma BN_\gamma \qquad (3.1)$$

where

$c = Cohesion$

$q = Sorrounding\ load$

$\gamma = Bulk\ density\ of\ the\ soil$

$B = Width\ of\ the\ raft$

$N_c, N_q, N_\gamma = Bearing\ capacity\ factors$

The bearing capacity factors are functions of the friction angle. The factors have been derived analytically by several researchers, with different results. According to [3] the most commonly used solution for N_c, N_q, N_γ are

$$N_q = \tan^2\left(\frac{\phi}{2} + \frac{\pi}{4}\right)e^{\pi\tan(\phi)} \qquad (3.2)$$

$$N_c = \frac{(N_q - 1)}{\tan(\phi)} \qquad (3.3)$$

$$N_\gamma = 1.5(N_q - 1)\tan(\phi) \qquad (3.4)$$

The general bearing capacity equation is valid for a raft, which is long, has a horizontal base, located at the ground surface and is vertical loaded [3]. For other cases there is a modified bearing capacity equation with empirical correction factors, which governs other geometries.

3.2.2. Settlement

The settlement beneath the raft could be calculated as

$$s = \int_z \varepsilon dz = \int_z \frac{\Delta\sigma'_z(z)}{M_z(z)} dz \qquad (3.5)$$

Where $\Delta\sigma'_z$ is the induced stress and M_z is the compression modulus of the soil

Induced stress

The induced stress decreases due to load spread. There are some different models to describe the distribution of induced stress, as the Boussineq's method and the 2:1 method.

Compression modulus

The stiffness properties of clay are generally determined by a CRS-test, i.e. an oedometer test with constant rate of strain. A typical result from a CRS-test is illustrated in Figure 3.1, the doted line illustrate the moduli used in swedish praxis for settlement calculation.

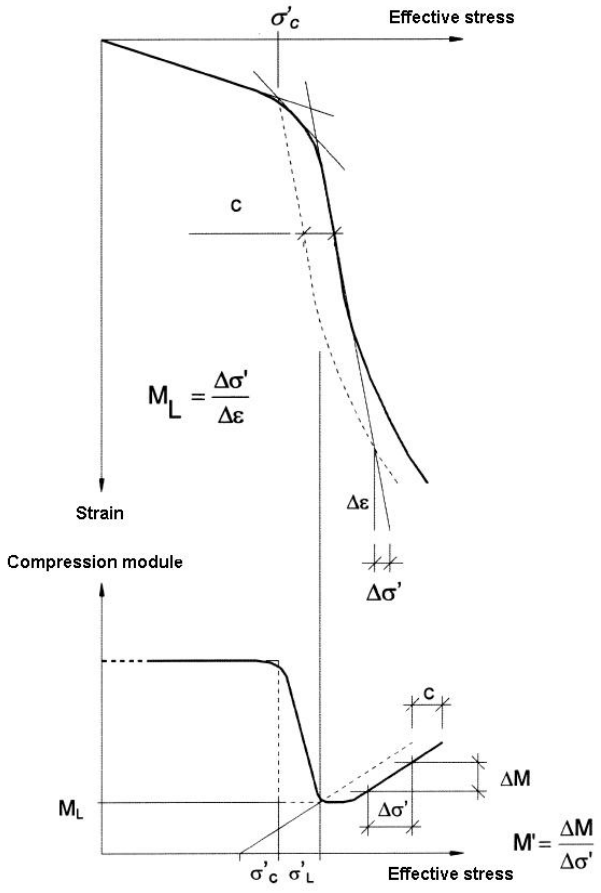

Figure 3.1. Typical CRS test result [4].

From a CRS-test, three stiffness moduli are defined in swedish praxis; M_0, M_L and M'. Where, M_0 is the stiffness modulus for stresses below the pre consolidation pressure σ'_c, i.e. the largest stress the soil has been exposed to. In this state the soil is called over consolidated.

M_L is the modulus for stresses above the pre consolidation pressure to σ_L (defined in the figure), in this stress range the soil is called normal consolidated. For stresses above σ_L the stiffness modulus starts increasing linear with the rate of M'. Soil compressed in a CRS-test behaves stiffer than the soil compressed in nature, this is due to inadequate consolidation time during the test. By moving the curve to the left one accounts for this fact.

This relation is suitable for hand calculations. However the relations between stress and strain could be modelled in various ways and this is further examined in Chapter 4.

Consolidation
The settlement in a soil with pore water is time-dependent. Since water is incompressible, the settlement is dependent on drainage of the pore water, this process is called consolidation. Clay has low permeability and thus a time-consuming consolidation. The consolidation is considered to be outside the scope of this thesis, and only the final total settlement is governed.

3.3. Cohesion piles

3.3.1. Bearing capacity

The bearing capacity of a pile is the minor of the structural capacity and the geotechnical capacity. This dissertation focuses on the geotechnical capacity, as mentioned earlier.

Single pile
The bearing capacity for a single pile is the sum of its shaft bearing capacity and its end bearing capacity [5]

$$R = f_{shaft} A_{shaft} + f_{end} A_{end} \qquad (3.6)$$

where, f_{shaft} is the friction strength at the interface between the soil and the shaft, and A_{shaft} is the shaft area. Further, f_{end} is the compressive strength of the soil at the toe of the pile at ground failure, and A_{end} is the cross section area of the pile at the toe.

In soft clays [4] recommends using the semi-empirical method called α-method to determine the bearing capacity for a pile, i.e.

$$R = f_{shaft} A_{shaft} + f_{end} A_{end} = \int_{L_p} \alpha c_u(z) \theta \, dz + N_c c_u A_{end} \qquad (3.7)$$

where

$\alpha = Interaction\ factor$
$\theta = Pile\ perimeter$
$L_p = Pile\ length$
$c_u = Undrained\ cohesive\ strength$
$N_c = Bearing\ capacity\ factor$

The interaction factor depends on; the pile perimeter, the pile shape, the OCR and also the time after installation [4]. Whiles [5] mention; the clay type, the shear strength, the OCR and the pile length. The following equation for determination of the interaction factor is recommended in [4].

$$\alpha = \kappa_\phi \kappa_s \kappa_{OCR} \kappa_T \qquad (3.8)$$

where

$\kappa_\phi = Pile\ perimeter\ reduction\ factor$

$\kappa_s = Pile\ shape\ reduction\ factor$

$\kappa_{OCR} = OCR\ reduction\ factor$

$\kappa_T = Time\ after\ installation\ reduction\ factor$

κ_ϕ is 0.9 for standard Swedish concrete piles and κ_s is 1 for constant cross sections [4]. According to [5], the mobilised strength decreases with an increased over consolidation ratio, as could be seen in Figure 3.2, from which κ_{OCR} is determined. When driving piles in soft clay the adjacent soil will be disturbed and a preliminary reduction of the shear strength around the pile occurs. The pore pressure will increase during installation and the reduced shear strength will regress as the excess pore pressure dissipates. This is governed by κ_T, which is determined by Figure 3.2. The driving process also is expected to create a gap between the pile and the soil in the upper zone, and therefore [4] and [3] advise one to set the interaction factor to zero for the upper 3 meter.

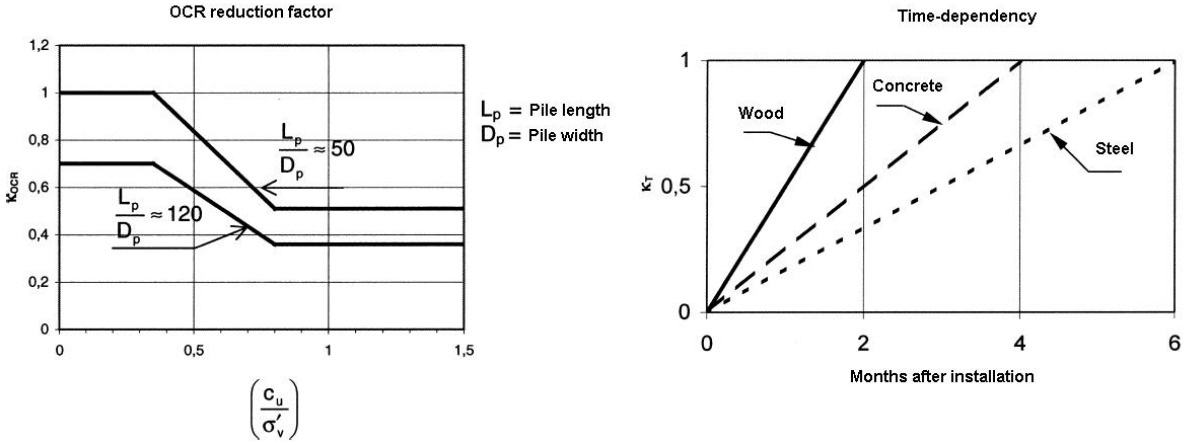

Figure 3.2. κ_{OCR} and κ_T respectively, based on [4].

The bearing capacity factor in Eq. 3.7 has experimentally been determined to 9.0 [4][5]. However, for piled raft foundation in deep layer of soft clay the end bearing resistance is often neglected. Since, the end bearing resistance requires rather large settlement to be mobilised, approximately 5-10% of the pile diameter compared to the shaft bearing resistance which requires 2-5mm to be mobilised [4]. Eq. 3.1 then could be modified to

$$R = R_{shaft} = \int_{L_p} \alpha \theta c_u(z) dz \qquad (3.9)$$

Pile group

Piles are often installed in groups. The interaction of the piles in the group are highly affecting the structure's load-settlement behaviour, this is illustrated in Figure 3.3. The interaction of piles depends on [6]; pile spacing, pile stiffness, shear strength in soil, homogeneity of soil and Poisson's ratio.

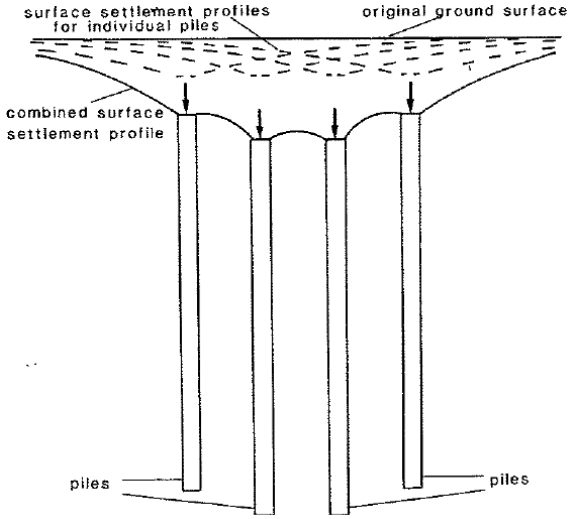

Figure 3.3. Pile group periphery [4].

If the piles are installed close together a special mode of failure could occur, i.e. the group could fail as a unit (block failure). With shear failure occurring at the periphery of the pile group, illustrated in Figure 3.4.

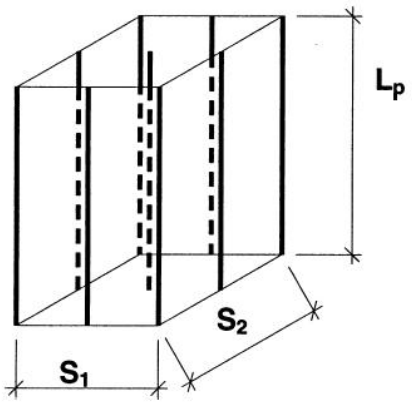

Figure 3.4. Pile group periphery [4].

Block failure will occur if the group resistance is less than the sum of the corresponding single piles resistance. This could be expressed as (for a rectangular pile group) [4]

$$2(S_1 + S_2)L_p c_u + N_c S_1 S_2 c_u \leq \sum_{i=1}^{n} R_i \qquad (3.10)$$

where

$S_1, S_2 = See\ Fig.\ 3.4.$

$R_i = The\ Single\ piles\ bearing\ capacity$

The bearing capacity factor should, for pile groups, be set to 6.0 according to [4]. But, as mentioned for single piles it is convenient to neglect the end bearing capacity, due to mobilise requirements.

3.3.2. Negative skin friction

In clays, reverse shaft friction can occur in the upper parts of the pile due to ongoing settlements, i.e. negative skin friction. These settlements could origin e.g. from; a fill placed on top of the clay, nearby structures, driving of piles or lowering of ground water. To mobilise strength or resistance the pile must move downwards relative to the soil, creating a frictional force upwards. In the case of negative skin friction the soil moves downwards relative to the pile and (instead of strength) a frictional load downwards is created, acting as an additional load. According to Swedish praxis the negative skin friction is calculated with the α-method, with $\alpha = 0.7$ [5], i.e.

$$F_{nskin} = \int_{L_{nskin}} 0.7\theta c_u(z)dz \qquad (3.11)$$

The neutral plane

The neutral plane is where the negative skin friction changes to friction strength. In this plane the movement of the pile and the adjacent soil are the same, thus no frictional stress occurs. The neutral plane could be found by solving the vertical equilibrium between force and resistance, i.e.

$$F = R \qquad (3.12)$$

Where F is the sum of the axial loading of the pile and the load caused by the negative skin friction. Leading to

$$F = F_{load} + F_{nskin} = F_{load} + \int_{L_{nskin}} 0.7\theta c_u(z)dz \qquad (3.13)$$

The total resistance R was expressed in Eq. 3.6. If the neutral plane is at the depth z, the equilibrium then take the form

$$F_{load} + \int_0^z 0.7\theta c_u(z)dz = \int_z^{L_p} \alpha\theta c_u(z)dz + N_c A_b c_u \qquad (3.14)$$

3.3.3. Settlement

The total settlement of a pile is the sum of three sub-settlements: compression of the pile element, slip between the pile and the ground, and the settlement in the ground. The first is often small, due to high axial stiffness in the pile. The slip between the pile and the ground is in general less than 5 *mm* [3]. The settlement in the ground is present below the neutral plane

where the load is transferred to the ground and could be calculated by assuming an equivalent footing at the neutral plane. The settlement beneath this equivalent footing could then be calculated using Eq. 3.5, as for a raft.

3.4. Pile-raft interaction

When analysing piled rafts the distribution of load carried by the raft and the piles must be determined. This interaction is very complex and is according to [5] dependent on; the superstructure's stiffness, the raft's stiffness, the stiffness of the piles, the soil's stiffness, fills, excavations and water pressure.

3.4.1. Different piled rafts

The interaction between the raft and the piles depend on the foundation design. Four different approaches are defined in [7], where the latter three is in the scope of piled raft foundation:

- The conventional approach, where the piles are designed for the entire load.
- Creep piling, in which the piles operate at 70-80% of their capacity, i.e. at the load where creep, typically, starts to occur. The piles are further used to limit the contact pressure below the pre consolidation pressure.
- Differential settlement control, where the bearing capacity of the raft is sufficient but piles are added strategically to reduce differential settlements.
- Settlement reducing, an extreme version of creep piling, in which the piles operate at 100% of their ultimate load capacity. The main purpose is to reduce settlement, rather than increasing the ultimate load capacity. But the ultimate load capacity is, of course, increased as well.

The load-settlement behaviour of the different versions is illustrated in Figure 3.5. Curve two corresponds to creep piling and curve three corresponds to using piles as settlement reducer. In the latter case the piles yield but the overall structure has a sufficient margin of safety and the settlement is also satisfying the settlement requirements. From this illustration one could do the conclusion that using piles as settlement reducer should be the most economical foundation design. This figure also illustrates the increase of bearing capacity when adding piles.

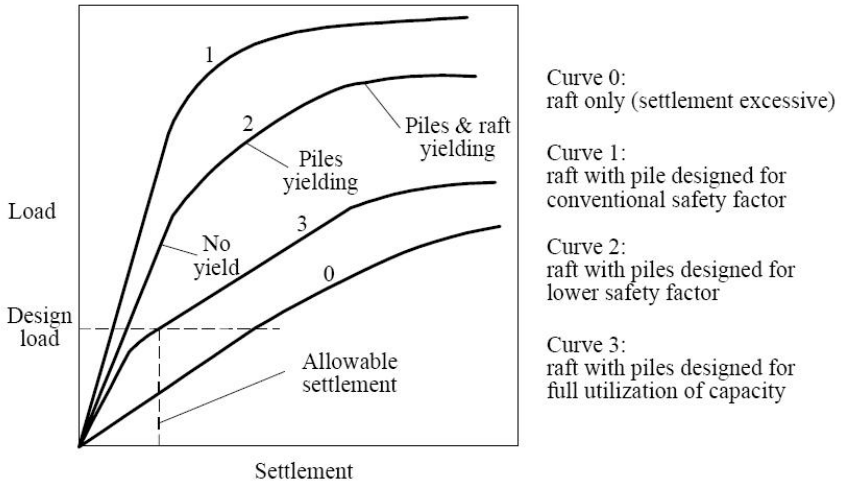

Figure 3.5. Different design approaches of piled raft [7].

The use of settlement reducing piles for uniform and concentrated loads is illustrated in Figure 3.6 and 3.7, respectively. These pictures show the benefit of adding piles strategically, concerning differential settlements.

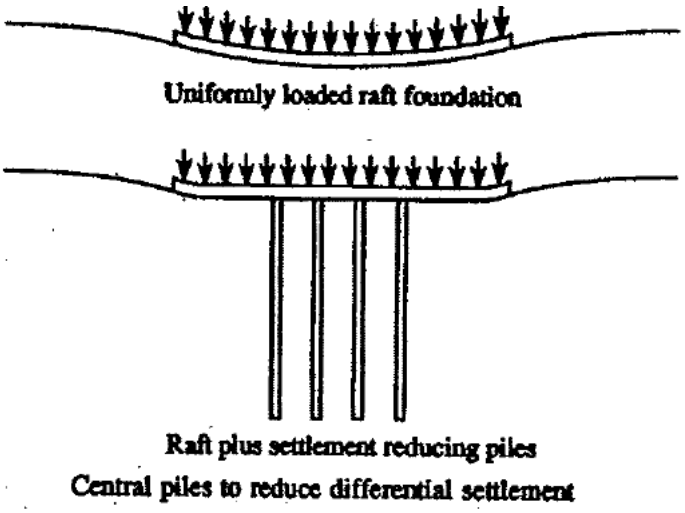

Figure 3.6 .Placing of the piles for uniform load [6].

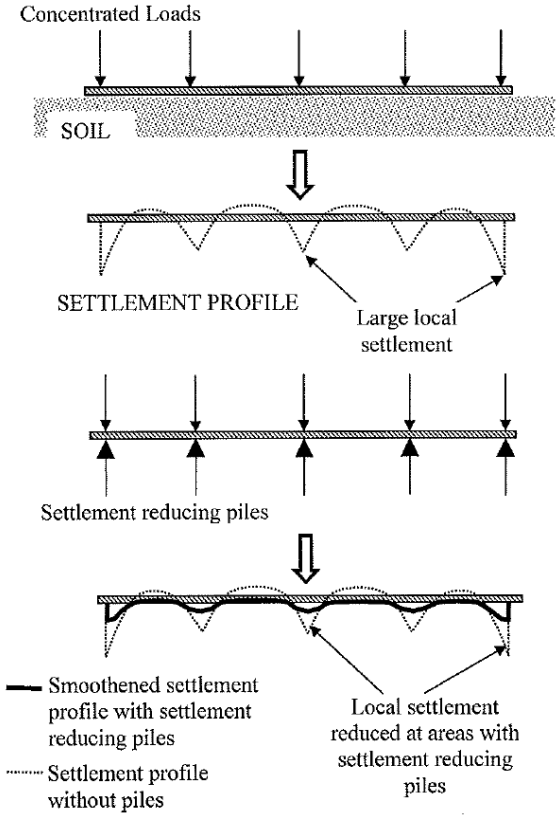

Figure 3.7. Settlement with settlement reducing piles, for concentrated load [6].

3.4.2. Methods of analysis

Several methods for analysing of piled raft foundation have been developed in the last decades, which all more or less take the pile-raft interaction into account. H.G. Poulos has in [7] evaluated several of the methods and divide them in three broad categories; simplified

calculation methods, approximate computer-based methods and more rigorous computer-based methods.

The simplified calculation methods are empirical methods with numerous simplifications, mostly concerning the soil profile and the load condition, e.g. Poulos-Davids-Randolph method. The approximate computer-based methods include various strip on spring and raft on spring methods, where the raft is modelled as a strip respective a plate, and the soil and the piles are modelled with springs with varying stiffness, e.g. using the Winkler hypothesis. The more rigorous computer-based methods consist of different numerical methods. In this dissertation focus is on the more rigorous computer-based methods. And four different models are examined; a full 3D FEM model and three plane strain models, all by using programs developed by Plaxis, i.e. Plaxis 3D Foundation and Plaxis 2D, respectivelly. Plaxis will be presented in the next chapter. Prior to that, the first plane strain method is described here. The two other plane strain models are analogous to this first plane strain model but they models the interaction between the piles and the soil in a different manner. These two alternative methods are described in Chapter 8.4 and 8.5 and are called AM1 and AM2.

Plane strain FEM-model for piled rafts

The main problem when modelling a piled raft with a plane strain model is the transition from three to two dimensions, i.e. to express a three dimensional problem in a two dimensional model. To do this the "out off"-plane rows of piles are simplified as wall elements, called plane strain piles (illustrated in Figure 3.8).

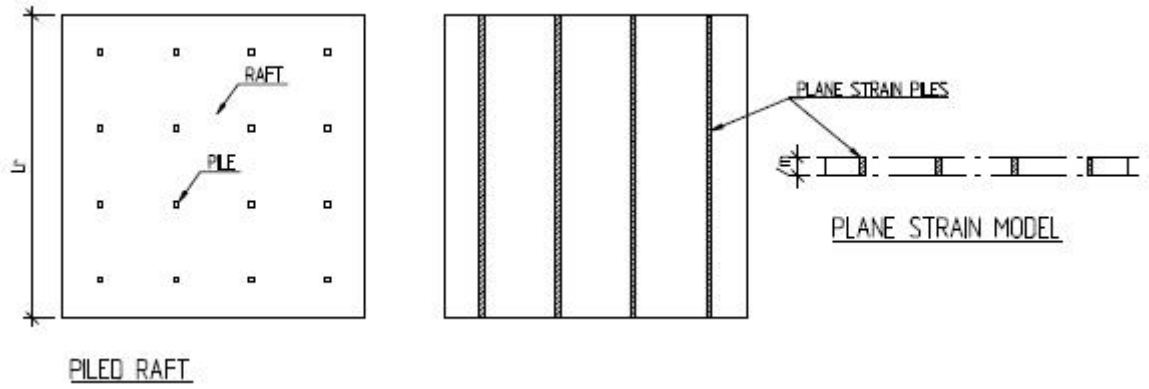

Figure 3.8. Plane strain model of piled rafts.

The wall element is defined per meter; the normal stiffness, bending stiffness and weight for the piles in the "out off"-plane row of piles are therefore "smeared" per meter

$$EA_{psp} = EA_p \frac{n_{p-row-i}}{L_r} \qquad (3.15)$$

where

EA_{psp} = *Normal stiffness for plain strain pile*

EA_p = *Normal stiffness for one pile*

$n_{p-row-i}$ = *Number of piles in row i*

L_r = *Raft length in plane*

Analogously, the bending stiffness is inputted as

$$EI_{psp} = EI_p \frac{n_{p-row-i}}{L_r} \qquad (3.16)$$

and the weight as

$$w_{psp} = w_p \frac{n_{p-row-i}}{L_r} \qquad (3.17)$$

The change of cross section when introducing the plane strain piles involves a change in periphery area, which will affect the important shaft resistance and an equivalent shaft resistance is therefore introduced. Since a plane strain pile has a periphery defined by its two sides, the shaft resistance is modified to [8]

$$f_{shaft,eq} = \frac{n_{p-row-i} A_s f_{shaft}}{2L_r} = \alpha_{ar} f_{shaft} \qquad (3.18)$$

where

$A_s = Shaft\ area\ \ per\ unit\ depth$

$\alpha_{ar} = Area\ ratio$

In Plaxis the plane strain piles are modelled by using plate elements with corresponding interface elements, where, the interface elements describe the interaction between the pile and the soil. This element is used to model the shaft resistance, as in [8]. Plaxis and the mentioned elements will be presented further in the next chapter. However, the interface element has the strength properties of the surrounding soil multiplied by a factor, called R_{inter} (i.e. strength reducing factor for interface). The shaft resistance is modified according to Eq. 3.18 by reducing the strength of the adjacent soil with the strength reducing factor, i.e.

$$R_{inter,eq} = \alpha_{ar} R_{inter} = \frac{n_{p-row-i} A_s}{2L_r} \qquad (3.19)$$

The change of cross section does also affect the end resistance but can not be modified in the plane strain model, since the cross section lack dispersion in the model. However, since the end resistance in general is small compared to the shaft resistance for floating piles, the effect is not significant [8].

Similar plane strain models were examined in [7] and also in [9], by comparing it to other analysis method for simple examples. The comparison showed that the plane strain models, may lead to over-estimation of the settlement and the pile force. Another study was presented in [8] has lead to the same conclusions with one addition, i.e. a general underestimation of the differential settlement. In this dissertation, a parametric study of different shapes and pile configurations of piled raft foundation is carried out, to study the behaviour of this model for different geometries, where the 3D-effects are expected to have varying impact.

4. Plaxis

4.1. Introduction

Plaxis is a Dutch company developing software, with the same name, that is using the finite element method (FEM) for modelling of geotechnical problems. The software portfolio includes two and three dimensional simulation of soil and soil-structure interaction. Plaxis governs three main theories in its FEM-code; deformation, groundwater flow and consolidation. Additional, there is an extension-program for dynamic calculations. In this thesis the versions; “Plaxis 2D Version 9” and “Plaxis 3DFoundation” have been used and only static calculation is covered.

In this chapter Plaxis is presented, first “Plaxis 2D”. Then “Plaxis 3DFoundation”, which has a lot in common with the 2D version, but of course important differences. Subsequently, the material models available in Plaxis are presented. This chapter is, if nothing else is stated, based on the Plaxis manuals [10][11].

4.2. Plaxis 2D

In Plaxis 2D it is possible to model geotechnical problems either in a plane strain condition or as an axisymmetric model. In this dissertation the problems are analysed using the plane strain alternative.

After specifying the model type, the general procedure when modelling in Plaxis is to; define the geometry with elements and corresponding materials, define loads and boundary conditions, create a FEM-mesh, define the initial condition, performer the FEM-calculation. The procedure is in this chapter explained more throughout step by step.

4.2.1. Geometry and elements

When creating a geometry one first define points, geometry lines and clusters (areas). These are later assigned different properties. The clusters are given a soil element and a soil material, a geometry line is given either a structural element or a boundary condition. The different elements available in Plaxis 2D are:

Soil element (Volume element)
There are two different elements implemented for soil modelling in Plaxis 2D. These are both triangular elements and have 6 nodes respective 15 nodes and have 3 respective 12 stress points (i.e. Gaussian integration points), see Figure 4.1.

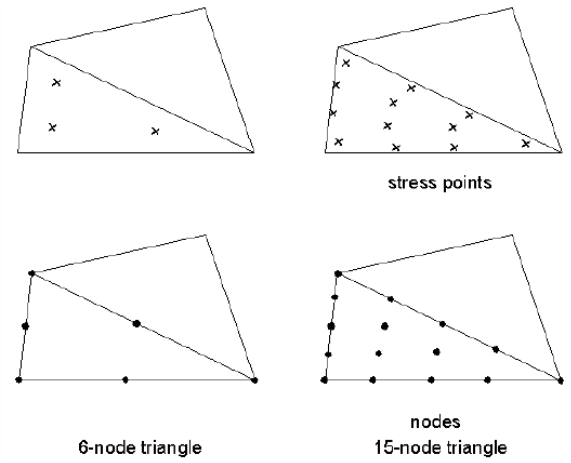

Figure 4.1. Soil elements [10].

The properties are assigned to a cluster and thereby a soil element is defined by the choice of material model. The material model is important when modelling soil and Chapter 4.4 is explicitly dedicated to this subject.

Plate element
The plate elements are in fact composed of beam elements. The beam element has three degrees of freedom per node and has three respective five nodes when used with 6 nodes volume elements and 15 nodes volume elements.

Mindlin's beam teory is implemented in Plaxis for this matter. This theory governs both deflection due to shearing and bending. It is also accounts for change in length when exposed to axial force.

The input parameters are; EA, axial stiffness, EI, bending stiffness, w, weight and v, Poisson's ration. One could choose elastic or elastoplastic behaviour. The latter requires two limit parameters for which plastic behaviour occurs, i.e. maximum bending moment and maximum axial force.

Geogrid element
Geogrid is an element, which only has tensile strength, i.e. no compressive strength or bending moment strength (as cables in structural mechanics). These are used for modelling of soil reinforcement with geotextiles, which often is used in geotechnical structures to add tensile strength in soil. Geogrids may also be used with node-to-node anchor for modelling of tie backs. Where the geogrid represents the grout and the node-to-node anchor represents the rod.

Interface element
Interface elements are used for modelling of the interaction between two materials. In FEM calculations just one displacement is allowed in a specific node. Hence, in a node common for two elements with different material properties one (or same) displacement must be present. Where soil meets structural elements this is unrealistic, one expects the soil to slip and also gap relative to the structural element, e.g. a pile slipping relative the surrounding soil due to external loads. This is governed in Plaxis by introducing the interface element, which has two

nodes for every stress point. In Figure 4.2 two interface elements are illustrated, with corresponding volume element.

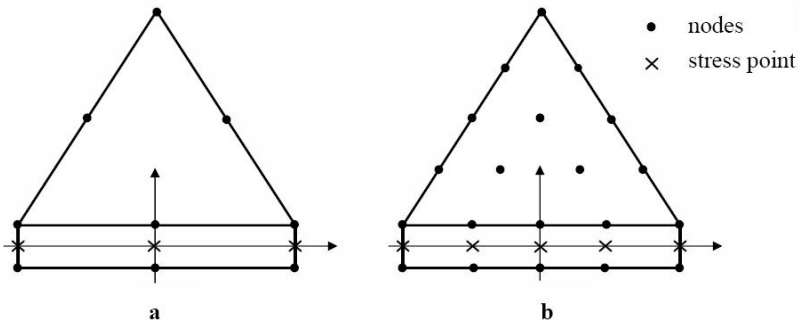

Figure 4.2. Soil element coupled to an interface element. When using 6-nodes element and 15-nodes element, respectively [10].

The interface element is described with an elastic-plastic model, where the Coulomb criterion (see Chapter 2.2) is used. The properties of the element are based on the corresponding soil. And the user could reduce (and increase) the strength of the interface with the strength reduction factor R_{inter}, according to

$$c_i = R_{inter} c_{soil} \tag{4.1}$$

$$\tan(\varphi_i) = R_{inter} \tan(\varphi_{soil}) \tag{4.2}$$

where c_i and φ_i are the cohesion and friction angle of the interface element. According to Plaxis R_{inter} is of the order 2/3 in most cases. The reduction is normally greater for cohesive soil than for frictional soil. According to [12] R_{inter} is in the span; 0.7-0.8 for cohesive soil and 0.9 for frictional soil.

The elastic slip and gap displacement is calculated by Plaxis as

$$Gap\ displacement = \frac{\sigma \cdot t_i}{E_{oed,i}} \tag{4.3}$$

$$Slip\ displacement = \frac{\tau \cdot t_i}{G_i} \tag{4.4}$$

where t_i is the virtual thickness of the interface element, $E_{oed,i}$ is the oedometer modulus of the interface element and G_i is the shear modulus for the interface element. These are defined as

$$E_{oed,i} = 2G_i \frac{1-0.45}{1-2 \cdot 0.45} \tag{4.5}$$

$$G_i = R_{inter}^2 G_{soil} \tag{4.6}$$

The material of the interface element could also be defined by creating a new material, specific for the interface element.

Another feature of the interface element is that it is impermeable. It could therefore be used in consolidation analysis and groundwater flow analysis to block groundwater flows. This feature is often used for preventing flow true plates, which are fully permeable in Plaxis.

The interface element could also be used to smooth the mesh around areas with high stress and strain gradient (e.g. sharp edges in stiff materials). Standard volume elements have difficulties to produce physical stress oscillation in such areas. Smoothening is created by applying interfaces around the area and active them during mesh generation, during calculation however these should be deactivated.

Anchor element
There are two anchor elements in Plaxis, node-to-node anchor and fixed-end anchor. They are both modelled as springs, with stiffness both in compression and tension. The first is a two node spring that models the ties between two points and the latter is a one node spring coupled to a fixed end. The input parameters for these elements are the position of the anchors and the stiffness, i.e. EA, and also the spacing between them.

4.2.2. Loads

Two types of load could be applied in this version, i.e. distributed load and point load, these could be applied in *x*- and *y*-direction. Since the model is two dimensional, the point load is in fact a one meter line load in the out-of-plane direction, i.e. N/m. Likewise, the distributed load has a thickness of one meter in the out-of-plane direction, i.e. N/m^2.

4.2.3. Mesh generating

Plaxis has implemented an automatic mesh generator developed by Ingenieursbureau SEPRA. This generates an unstructured mesh with the chosen type of element, either 6-node or 15-node element.

The user could choose from five different coarseness of the global mesh and could also make the mesh finer in local parts of the model. The latter option is a convenient way to ensure having sufficient elements in parts exhibiting great stress and strain gradients, without creating a heavy (i.e. time consuming) mesh.

4.2.4. Initial condition

Prior to the main calculations in Plaxis, the initial condition of the soil must be determined. This includes calculating both the initial effective stress-state and the initial water pressures in the soil.

Water pressures
In Plaxis the initial water pressures could be generated in two manners, either directly from the phreatic level or by a steady state groundwater calculation. In both methods the user must define the phreatic levels and in the latter it is possible to prescribe the groundwater head or discharge (only possible to set the discharge to zero). The groundwater calculation is based on

the finite element method and uses the generated mesh, the permeability of the soil and the boundary conditions to calculate the water pressures.

Effective Stress
The initial stress state is in a two dimensional analysis defined by the vertical stress together with the horizontal stress. As mentioned in Chapter 2 the vertical stress is caused either by external load or by the deadweight of the soil and the horizontal stress could further be calculated with knowledge of the coefficient K. Plaxis calculates this two stresses in every stress point in the model for an initial conditon. The initial condition implies no external loads and the vertical stresses are therefore calculated using the soils unit weight. The initial condition also implies the soil being at rest. The horizontal stresses are therefore calculated using the at-rest coefficient of lateral earth pressure, i.e. K_o. The default value of this coefficient is $K_o = 1 - \sin(\varphi)$ (Karky's formula), but could also be chosen by the user.

4.2.5. Calculations

When the geometry is set and the initial conditions are calculated, one could perform the main FEM calculation. There are three different types of calculations available for this matter, i.e. plastic calculation, consolidation calculation and safety calculation. Additionally it is possible, in all types, to account for large displacements ("Updated mesh") and also to perform dynamic calculations with an extension-program, neither of these features is regarded in this dissertation. The different calculation types are presented here.

Plastic calculation
Plastic calculation is for elastic-plastic deformation calculations. It is used when failure and stability of the object are analysed. Plastic calculation does not account for the time-dependent decay of excess pore pressure, and is therefore not appropriate when analysing settlement in low permeable soil. On the other hand, the calculation type could be used when calculating settlement in high permeable soil or when the final settlement of a structure is calculated.

Consolidation analysis
Water-saturated soil must drain water to develop settlement (due to waters incompressibility). In low permeable soil, such as clay, this is a time-consuming process and it is important to account for this process when analysing settlement. That is governed in the consolidation calculation. Hence, this calculation type is suitable for analysing time-dependent settlement for water-saturated and low permeable soil.

Safety analysis (PHI-C Reduction)
For safety analysis (i.e. calculating the safety factor), Plaxis has implemented a calculation type called PHI-C Reduction. This is a plastic calculation where the strength parameters for soil and interfaces are reduced until failure. The safety factor for the object is then calculated as the available strength divided by the strength at failure. Designing and safety factors are not in the scope of this work.

Staged Construction
A construction is, in practice, built in stages. To resemble and simulate this, the calculation process in Plaxis is also divided into stages, called calculation phases. This is mainly to avoid failure during construction and to simulate excavation processes.

The first calculation phase is always the earlier defined initial condition. One could then add an adequate number of phases where structural objects, loads and soil-clusters are activated or deactivated, successively, according to the planned construction process. It is also possible to change material data and the water condition and also to pre-stress anchors.

4.2.6. Results

When the calculations are finished, Plaxis supplies the user with several different illustrations of the stress and deformation distribution. This is done in two different programs called Output and Curves. The Output program illustrates the stress and deformation distribution by arrows, contour lines or shades. The user is also provided with the final stresses and deformation for all nodes in tables. In the Curves program the user is provided with curves and tables of the variation of displacement in specific points (chosen by the user).

4.3. Plaxis 3DFoundation

3DFoundation is a three dimensional finite element method software for deformation analysis of foundation structures. The general work process in 3DFoundation reminds of the work process in Plaxis 2D. This section intends to highlight the main differences between Plaxis 3DFoundation and Plaxis 2D.

4.3.1. Geometry

In 3DFoundation the geometry is defined by vertical “boreholes” and horizontal “work planes”. The boreholes are used to define the soil’s cross section, the ground surface level and the pore pressure distribution. And the work planes are used to define geometry points, geometry lines, clusters, loads, boundary conditions and structures.

Boreholes
When creating a geometry model it is recommended to start defining the boreholes and thus the vertical depth of the model. Vertical is defined as the *y*-direction. The boreholes are divided in layers, which subsequently are assigned different materials (i.e. different soil properties). When multiple boreholes are present in the model, the soil properties are interpolated between the boreholes thus creating non horizontal soil layers.

The pore pressure distribution is defined in the boreholes. The distribution could be entered manually or (if a hydrostatic distribution is expected) be generated from the phreatic level (defined by the user).

Work planes
A work plane is a horizontal plane (defined as *xz*-plane) at a certain depth, in which the horizontal geometry is defined. At least two work planes are required to create a geometry model but several could be defined if the horizontal geometry varies with depth. However, if a new point or a new geometry line is defined in a work plane the same point or geometry line is also created in the other work planes, i.e. all work planes have the same “structure”. One

first defines points and geometry lines, which then automatically divide the plane in clusters. Subsequently, structural objects, loads and boundary conditions could be assigned to the work plane. One must also assign a material to the structural object, as in Plaxis 2D. The work planes could be used to simulate construction phases and excavations. When defining the work planes, care must therefore be taken to geometries that will arise during the later calculation process.

4.3.2. Elements

The elements in Plaxis 2D are also available in 3DFoundation. These are of course modified in respect of number of nodes, number of stress points and number of degrees of freedom, due to the added dimension. This could be seen in Figure 4.3, where the volume element in 2D and 3D is compared. Plaxis has also changed the names of the elements e.g. the plate element is in 3DFoundation called floor and wall element, depending on orientation. The modified and renamed elements, earlier presented in Plaxis 2D, will not be presented further. However, there are two new pile elements in 3DFoundation, called volume piles and embedded piles, which are presented here.

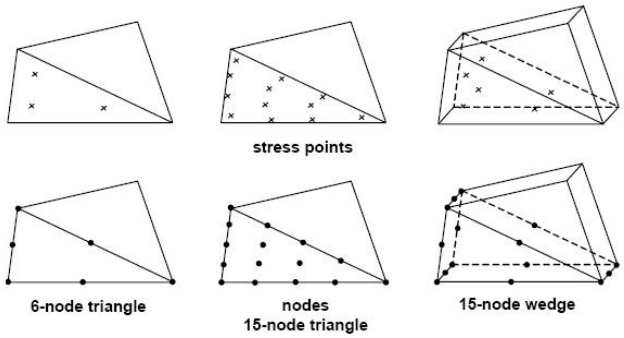

Figure 4.3. Comparison of two and three dimensional volume elements [10].

Volume piles

The geometry of the volume piles is defined vertically by specifying two work planes, between which, the piles should be drawn. The piles are then defined horizontally by choosing a cross section. There are five different cross section types available; massive circular pile, circular tube pile, massive square pile, square tube pile and user-defined shape pile. The tube piles (i.e. hollow piles) are composed of wall elements and the massive piles are composed of volume elements. The material properties are subsequently assigned to the piles. All pile types have interface elements (optional), which are placed at the periphery of the piles. These are implemented to model the interaction between the piles and the surrounding soil, such as the shaft resistance. The interface element is defined by the reduction factor R_{inter}, as in Plaxis 2D.

Embedded piles

Embedded piles are beam elements with a special interface element (for pile-soil interaction). The embedded piles could be placed in an arbitrary direction and are thus convenient for analysis of inclined piles. The input parameters for an embedded pile are; pile stiffness, unit weight, pile cross section and R_{inter} (divided in shaft and end resistance). Another feature of this element is the possibility to specify the stiffness of the pile top connection.

4.3.3. Loads

In 3DFoundation the loads are, unlike Plaxis 2D, inserted without simplifications, i.e. as distributed loads, line loads and point loads, in an arbitrary direction.

4.3.4. Mesh generation

The general process when generating a FEM mesh in 3DFoundation is to first generate a 2D mesh for the work planes, similar to the mesh generation in Plaxis 2D, then to generate a vertical mesh. The vertical mesh connects the work plane meshes together, with account taken to the soil profile defined in the bore holes. If non-horizontal soil layers are present, some volume elements may be degenerated from 15-node wedge elements to 13-node pyramid elements or 10-node tetrahedral elements. The number of element highly influences how time-consuming the calculation will be, Plaxis therefore recommend the user to avoid very dense 2D meshes, since they will lead to a large amount of 3D elements.

4.4. Material models

Soil is a non-linear, multi-phase, stress-dependent and time-dependent material. Hence, the material model, i.e. the constitutive relation between stress and strain, is very complex. The constitutive relation can be modelled more or less accurate and with focus on different features. Plaxis has implemented eight different material models, suitable for different cases. These models are presented in this chapter, with focus on the one used in the present work.

4.4.1. Liner elastic model (Hooke's law)

Hooke's law is a linear elastic and isotropic relation between stress and strain. This constitutive relation is the simplest material model implemented in Plaxis. It involves two input parameters; Young's module, E, Poissons ratio, v. This model is not suitable for modelling of soil, due to soil's complex behaviour. Hooke's law is on the other hand a good idealisation for material in structural elements, such as steel, which often behaves linear-elastic and isotropic, at least in its lower stress states.

4.4.2. Mohr-Coulomb's model

The Mohr-Coulombs model (MC-model) is an elastic perfectly-plastic model. The general behaviour of an elastic perfectly plastic material is illustrated in Figure 4.4. The model requires five input parameters; E and v for the elasticity, φ and c for plasticity and ψ for the dilatancy. The model is isotropic and does not account for soils stress-dependency, i.e. soils tendency to stiffen with increased pressure. Plaxis recommend using this material model in an initial simulation of soil because it is relatively fast and fairly accurate.

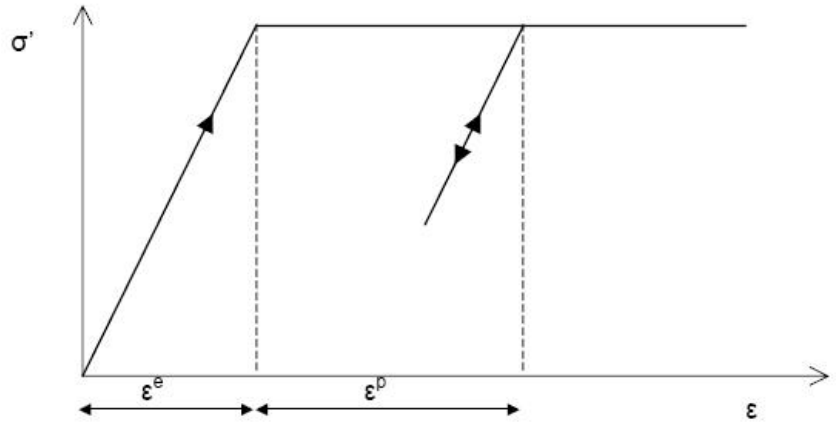

Figure 4.4. Basic idea of an elastic perfectly plastic model [10].

Plasticity and Yield functions

When modelling plasticity Plaxis introduces functions called yield functions, which are equal to zero when the material behaves plastic. The Mohr-Coulomb yield condition consists of six yield functions, all expressed with principal stresses, the friction angle and the cohesion. The Mohr-Coulomb yield condition is an extension of the Coulomb friction law and obeys this law in any plane within the material. When the six functions are set to zero (i.e. acting plastic) they create a surface in the principal stress space called the yield surface, illustrated in Figure 4.5. When the material is exposed to stress states within this surface it acts elastic and Hooke's law obeys.

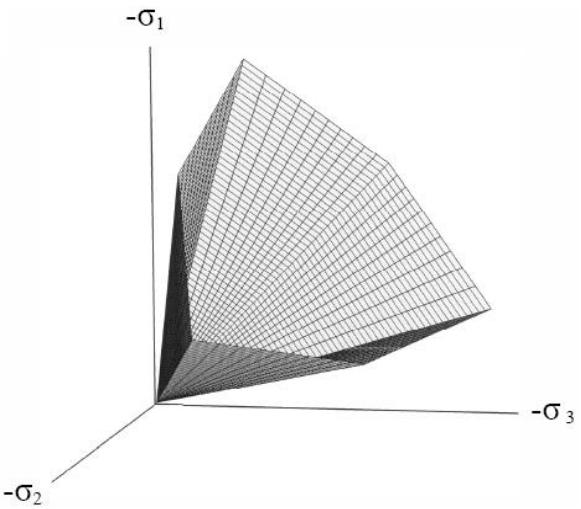

Figure 4.5. Mohr-Coulombs yield surface in principal stress space [10]

Perfectly plastic means that the constitutive relation is independent of the plastic strain and fully defined by the model's input parameters. This leads to a fixed yield surface. In contrast, more advanced models that are plastic, not perfectly-plastic, have a yield surface that expands due to plastic strain.

Input parameters

When prescribing soil's stiffness Plaxis recommend using E_{50} as stiffness when modelling initial loading and E_{ur} when modelling unloading and reloading problems as excavations.

Where E_{50} is the Young's modulus at 50% of the maximum stress-level occurred in a triaxial test and E_{ur} is the Young's module for soil when unloading and reloading. The latter is normally higher than for initial loading since the soil stiffens due to increased stress-level.

When *v* is unknown Plaxis recommends using values in the range 0.3 to 0.4 and 0.15 to 0.25 for loading scenarios and reloading scenarios, respectively.

When modelling sand without cohesive strength Plaxis will not perform well numerical. The cohesion should therefore be prescribed to a small value, in the order of magnitude $c \approx 0.2kPa$.

The computing time increases exponentially with increasing friction angle [10]. Hence, one should avoid prescribing high values for the friction angle when doing rough time-limited calculations.

According to [10] the dilatancy angle for sand with high friction angle is roughly $\psi = \varphi - 30$. For sand with less friction angle than 30° and for clay the dilatancy is close to zero [10].

Advanced input parameters
In addition to the five input parameters mentioned above three advanced parameters can be set; increase of stiffness, increase of cohesion and tension cut-off.

Increase of stiffness involves soil's stress-dependency by introducing $E_{increment}$ and y_{ref}, i.e. increase of stiffness per meter and the depth where the increase starts, respectively. In an analogous way the cohesion could be increased with depth in "increase of cohesion".

Tension cut-off implies prescribing soil's tensile-capacity to zero. The basic Mohr-Coulomb model has this option as default. Tension cut-off is suitable for most soils, such as sand and gravel with no tensile strength. However, in clay it could be adequate to account for tensile strength and tension cut-off could then be deactivated.

4.4.3. Jointed rock model

Jointed rock model is, as the Mohr-Coulomb model, elastic perfectly plastic. The model is anisotropic and specially made for analysis of stratified and jointed rock layers. Hence, this model is not in the scope of this work and is not discussed further.

4.4.4. Hardening-soil model

Hardening-soil model (HS-model) is an advanced model behaving isotropic and hardening plastic. It models the soil's stiffness, hardening process and plasticity more accurately than the Mohr-Coulomb model.

Hyperbolic relation
The relation between stress and strain is in this model explained by hyperbolic curves which have been derived from standard triaxial tests, such a relation is illustrated in Figure 4.6. The failure line in the figure is derived from the Mohr-Coulomb failure criterion.

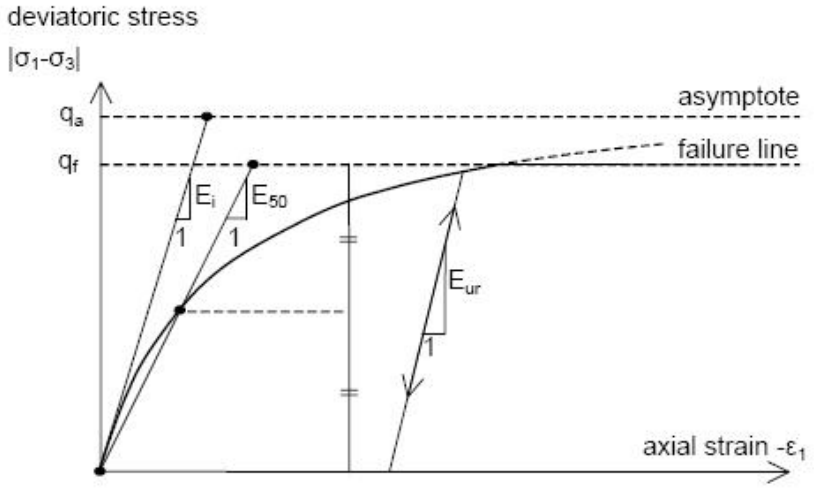

Figure 4.6. The cap yield surface in principal stress space [10]

Plasticity and Yielding

In contrast to the earlier mentioned models, which are elastic perfectly-plastic, the Hardening-soil model has a yield surface that expands due to plastic strain, thereby describing the plasticity more realistic.

Plastic volumetric strain has been observed in soil exposed to isotropic compression [10]. The yield surface described until now does not account for this phenomenon. Plaxis has introduced a second surface, illustrated in Figure 4.7, closing the elastic region which governs this behaviour. This cap is dependent on the friction angle, the odometer module and the pre-consolidation.

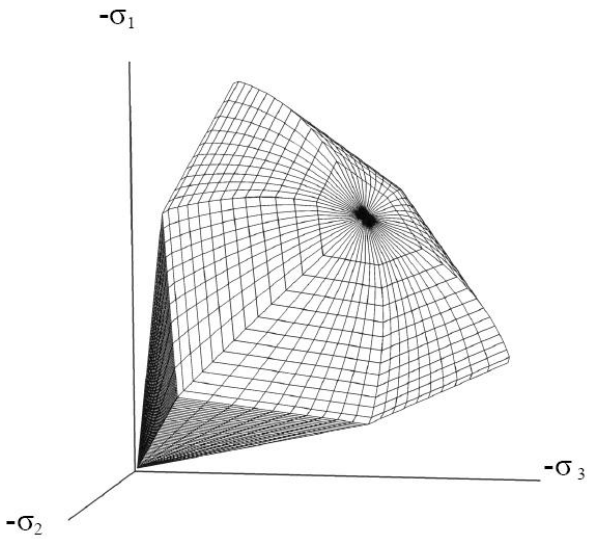

Figure 4.7. The cap yield surface in principal stress space [10]

Input parameters

The model describes soils stiffness with three Young moduli E^{ref}_{50}, E^{ref}_{ur} and E^{ref}_{oed}, i.e. the triaxial primary loading stiffness, triaxial unloading/reloading stiffness and the oedometer primary loading stiffness, respectively.

The soil stiffness is also modelled as stress-dependent, i.e. hardening with increased pressure. This is ruled with a parameter m coupled to power law, which span from 0.5 to 1. Values of 1 for soft clays, and 0.5 for Norwegian sand and silt, are mentioned in the manual. The stress dependency is a big advantage compared with the Mohr-Coulomb model, since soil is highly stress-dependent.

The soil's pre-consolidation is also taken into account in the HS-model. It is governed in the initial stress calculation and is specified by the over consolidation ratio (OCR) or the pre-overburden pressure (POP), which is defined as

$$OCR = \frac{\sigma'_p}{\sigma'_{vertical}} \tag{4.7}$$

and

$$POP = \left|\sigma'_p - \sigma'_{vertical}\right| \tag{4.8}$$

where, σ'_p is the pre-consolidation pressure, and $\sigma'_{vertical}$ is the in-situ effective vertical stress. OCR and POP are illustrated in Figure 4.8.

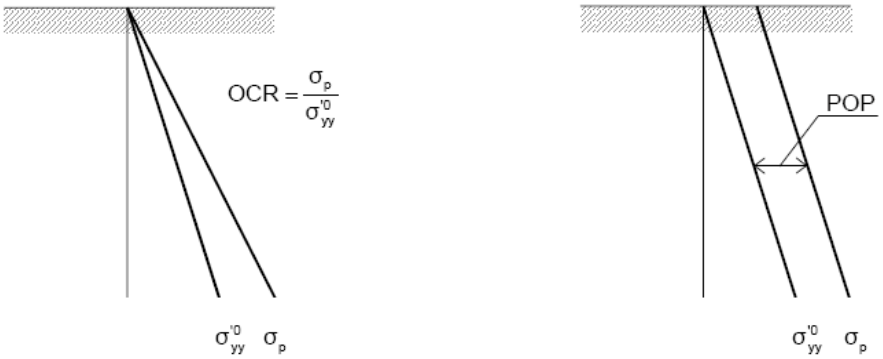

Figure 4.8. Definition of OCR and POP [10]

The soil's failure properties are described with c, φ and ψ, as in the Mohr-Coulomb model.

4.4.5. Hardening-soil model with small-strain stiffness (HSsmall)

This model is, as the name indicates, a version of the Hardeing-soil model. Hardening-soil model with small-strain stiffness (HSsmall-model) is a more advanced version, with focus on describing soil's behaviour more accurately while unloading and reloading the soil. The original HS-model models the stress-strain relation in this phase as linear-elastic with the stiffness E_{ur}. However, when a normally consolidated soil is unloaded and reloaded it will behave nonlinear and plastic, illustrated in Figure 4.9 for a typical soil. The HSsmall take account for this behaviour.

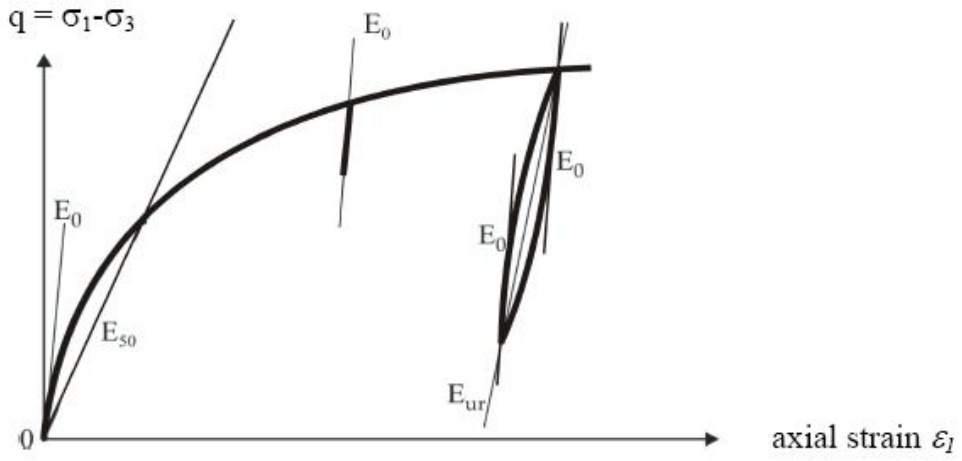

Figure 4.9. Unloading and reloading in triaxial test [10]

4.4.6. Soft-soil-creep model

The earlier mentioned Hardening-soil model is suitable for all soils including soft-soil. But the HS-model does not account for creep, i.e. secondary time-dependent settlements. This is a phenomenon highly influencing the settlements in soft-soil, i.e. normally consolidated clay, clayed silt and peat, when subjected to high primary compression. Soft-soil-creep model is focused on this phenomenon and is therefore suitable for long-time settlement calculation in soft-soil. This dissertation is limited to final settlement and this model will not be used.

4.4.7. Soft-Soil model and Modified cam-clay model

This model is an old model meant for modelling of primary compression in soft-soils. According to Plaxis this model is superseded by the HS model and is only kept for old users, who are comfortable with it. The modified cam-clay model is a new model for analysis of near normally consolidated clay-types soil.

5. Plaxis 2D Example 1 - Sheet pile wall

5.1. Introduction

In 2008 a building was built at Matrosgatan in Malmö. The building was founded with a basement, which implied an excavation. The property and the excavation where close to an existing road (Matrosgatan), a sheet pile wall was therefore installed. The sheet pile wall was designed as a cantilevering wall and should thereby be mounted to the firm rock. Problems during the construction lead to insufficient connection with the rock. Ramböll Sverige AB was hired to analyse the wall with the new characteristics and the characteristics were obtained from the responsible geotechnical engineer [12]. In this chapter the sheet pile wall is analysed to get a better understanding of Plaxis and soil-structure interaction, prior to the comparison of 2D and 3D modelling of piled rafts in Chapter 6-8.

5.2. Characteristics

The soil cross-section at the site was idealised by [12], according to Table 5.1.

Table 5.1. Soil cross-section AMSL= Above mean sea level.

Layer	Upper AMSL	Lower AMSL	Thickness	Unit
Fill	+2.2	-1	3.2	m
Moraine Clay	-1	-7	6.0	m
Eroded Limestone	-7	-	-	m

The water table was situated 1.5 meter below the ground surface, and the excavation was kept dry using pumps. A point load of 80 kN was acting nine meters from the wall, due to concrete trucks. The point load was spread by a three meter wide steal plate. The excavation was 4.8 m deep and supported by AZ 50 sheet piles (AZ 50 from [13]). The piles were driven to the depth of 8.8 m and no interaction with the bedrock is assumed.

To control the stability of the sheet pile wall, the deflection where measured regularly during the excavation. A deflection of 180 mm horizontally was measured at the top of the sheet pile wall for the given section [12].

5.3. Model

5.3.1. Geometry

The geometry is presented in Figure 5.1.

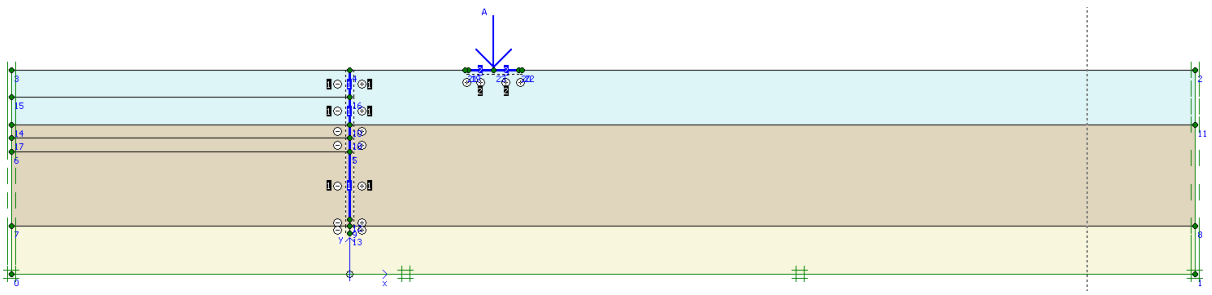

Figure 5.1. Geometry.

The model is 70x12 m^2. The displacements are prescribed to zero in both *x*- and *y*-direction in the bottom and only in the *x*-direction at the sides. The width of the model was derived by iteration, i.e. it was increased until the result was somewhat independent of the width.

The width of the model is chosen so that the boundary conditions did not o not introduce constrain, this was controlled by observing a normal shear stress distribution at the boundaries [12].

The clusters were arranged so that the excavation process could be simulated, using a staged calculation. The cluster's thickness is decreasing as the excavation depth increases, to prepare a stable calculation.

Three different elements are present in the model; 15-node element for the clusters, plate element for the sheet pile wall and the steal plate, and interface element for the interaction between the soil and structural elements.

5.3.2. Material properties

The soil was modelled with two material models; first with the Mohr-Coulomb model and then with the Hardening soil model. The MC model was mainly performed to quickly get a sense of the model, and the HS model to account for the stiffer behaviour when excavating. The input parameters used in the MC model are [12]:

Table 5.2. Material parameters for the soil layers

Input Parameter	Fill	Moraine	Limestone	Unit
Young's module, E'_{ref}	10000	35000	50000	kN/m^2
Poisson's ration, ν'	0.20	0.35	0.25	-
Saturated unit weight, γ_{sat}	20	21	20	kN/m^3
Unsaturated unit weight, γ_{unsat}	20	21	20	kN/m^3
Cohesion, c'_{ref}	0.2	3.0	0.2	kN/m^2
Friction angle, φ'	30	32	38	°
Dilatancy angle, ψ	0	2	0	°
Interface reduction factor, R_{inter}	0.9	0.8	1	-
Horizontal permeability, k_x	1	0.01	1.5	m/day
Vertical permeability, k_y	1	0.01	0.5	m/day

where the interface reduction factors are based on the values mentioned in Chapter 4.2.1. In the MC model it is assumed that the moraine clay has tensile strength, thus tension cut off is deactivated.

The same input parameters were used for the HS model with three additional Young's moduli and an additional power parameter (*m*), as explained in Section 4.4.4.

Table 5.3. Additional parameters for the HSmodel.

Input Parameter	Fill	Moraine	Limestone	Unit
Triaxial stiffness, E^{ref}_{50}	10000	35000	50000	kN/m^2
Oedometer stiffness, E^{ref}_{oed}	12500	43750	62500	kN/m^2
Un/Reloading stiffness, E^{ref}_{ur}	30000	140000	150000	kN/m^2
Power, m	0.75	0.75	0.75	-

Where the stiffness modulus E^{ref}_{50} is the same as in the MC- model, the other two modules were conducted from this module as; $E_{oed} = 1.25E_{50}$ and $E_{ur} = 3E_{50}$ [12], since no data for these modules were available. Plaxis mentioned values for *m* in the range 0.5-1, the mean value is used in the model.

The sheet pile wall and the steal plate have the following properties, where cross section area, weight and moment of inertia were found at [13] and Young's modulus of $E = 210$ GPa and poisons ratio of 0.3 were assumed.

Table 5.4 Material parameters for the Sheet pile

Input Parameter	Sheet Pile	Steel Plate	Unit
Normal stiffness, EA	6760000	10500000	kN/m
Flexural rigidity, EI	254000	2188	kNm^2/m
Poisson's ratio, ν	0.3	0.3	-
Weigth, w	2.5	3.9	kN/m/m

5.3.3. Mesh generation

The mesh was defined as medium dense and refined around the sheet pile wall and refined further at the bottom of the wall, as large stress gradients are expected there. Interface elements are drawn beneath the wall to smoothen the mesh, which is recommended by Plaxis in areas with high stress and strain gradient. The same mesh was used in both models.

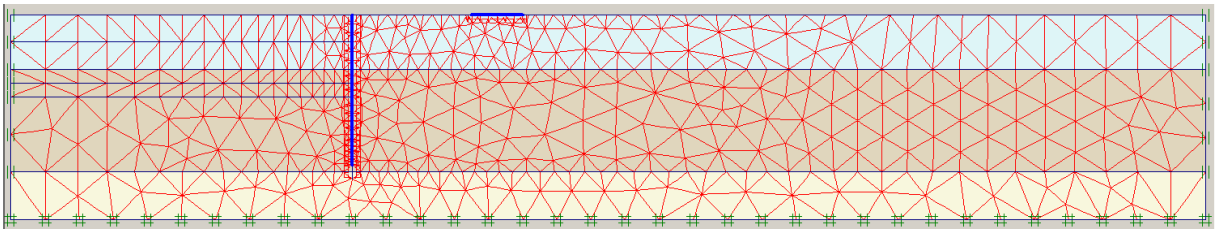

Figure 5.2. FEM Mesh.

5.3.4. Initial condition

The initial stress-state was calculated with the K0-procedure and the initial water condition was calculated by the direct method, using the phreatic level. For this calculation no elements were activated.

5.3.5. Calculation

The calculation was performed as a plastic calculation and with standard settings for the iterative procedure. The calculation was performed in seven stages to simulate the excavation process, these are; the initial phase which correspond to the initial condition, activating the plate element to simulate the pile driving, deactivating clusters in four stages to simulate the excavation, and finally applying the point load. For every excavation stage a steady-state groundwater calculation was performed, (i.e. to simulate the pumping) with a water table 0.1 meter beneath the excavation floor, to avoid numerical problems [12]. The interface elements were activated during the groundwater calculation to prevent flow through the wall.

5.4. Results

5.4.1. Stress distribution

The principal effective stress distributions are illustrated in Figure 5.3 and 5.4. When conducting the lateral earth pressure in Chapter 2.3, active and passive conditions were defined. By observing the major and minor principal stress, it is clear that the active condition rule behind the wall and the passive condition rule in front of the wall.

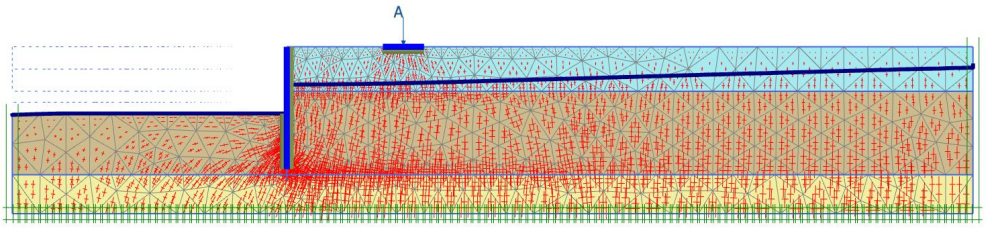

Figure 5.3. MC Principal effective stress.

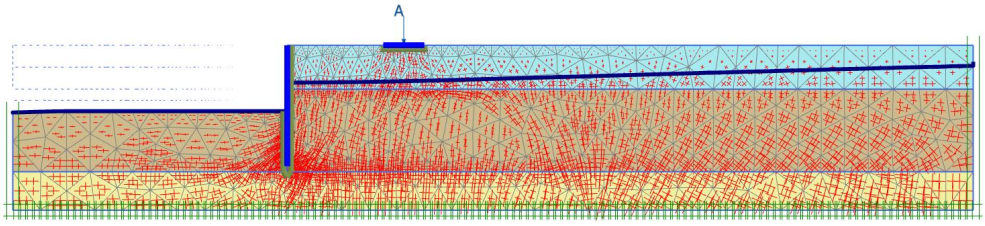

Figure 5.4. HS principal effective stress.

5.4.2. Deformation

The deformed mesh for the final stage is for the MC model and the HS model illustrated in Figure 5.5 and 5.6, respectively.

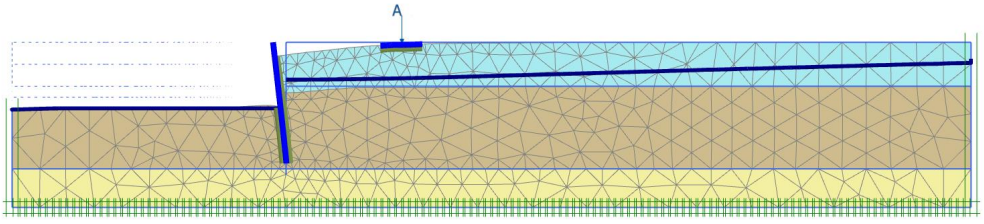

Figure 5.5. Deformed mesh in MC model.

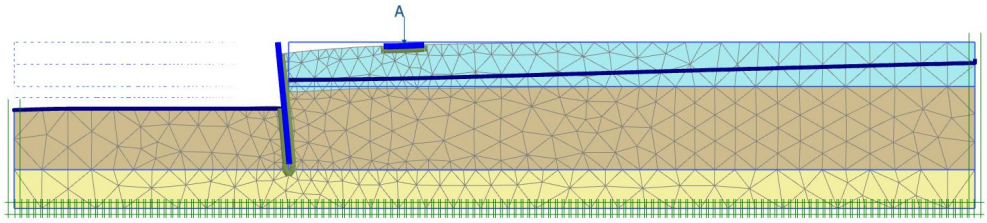

Figure 5.6. Deformed mesh in the HS model.

The horizontal displacements are illustrated with shades in Figure 5.7 and Figure 5.8 for the MC-model and the HS-model, respectively. The vertical displacements for the final stage is illustrated as shades for the MC model and for the HS model in Figure 5.9 and 5.10.

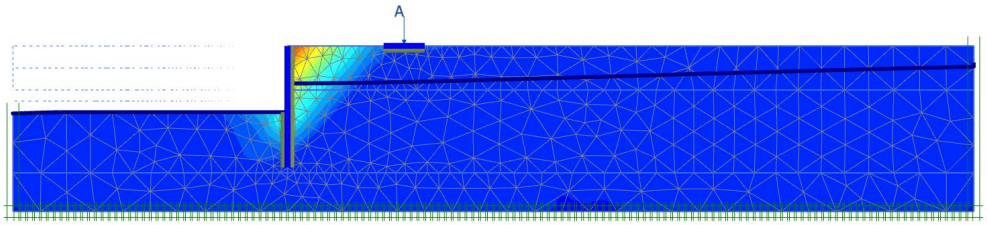

Figure 5.7. MC Horizontal displacement; max -185 mm.
Legend; red=-190 mm - blue=+10 mm.

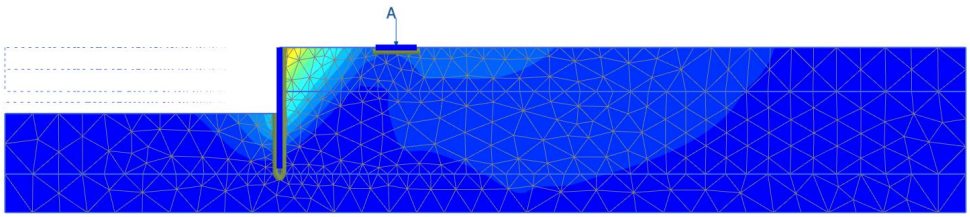

Figure 5.8. HS Horizontal displacement; max -155 mm.
Legend; red=-190 mm - blue=+10 mm.

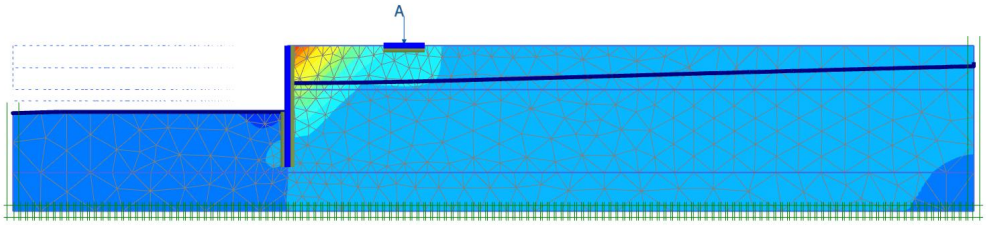

Figure 5.9. MC Vertical displacement; max -202 mm.
Legend; red=-220 mm – blue=+40 mm.

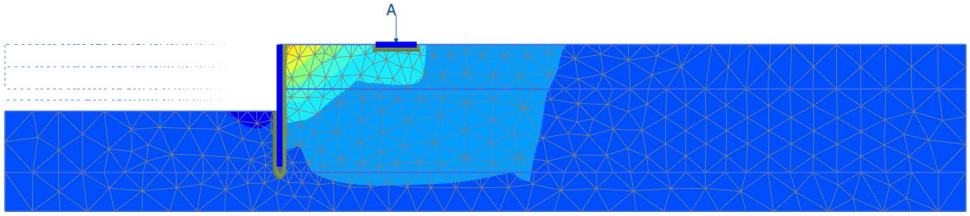

Figure 5.10. HS Vertical displacement; max -170 mm.
Legend; red=-220 mm - blue=+40 mm.

5.4.3. Forces in the wall

The axial force distribution, shear force distribution and bending moment distribution are illustrated in Figure 5.11 for the MC model and Figure 5.12 for the HS model.

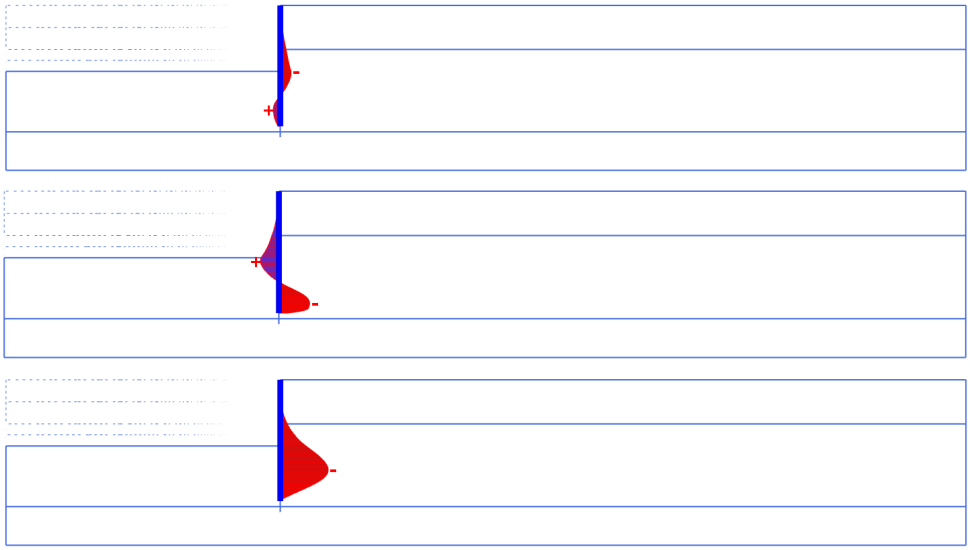

Figure 5.11. MC Forces in the sheet pile wall; axial force, max -40 kN/m , shear force, max -113 kN/m, bending moment, max -175 kNm/m, respectively.

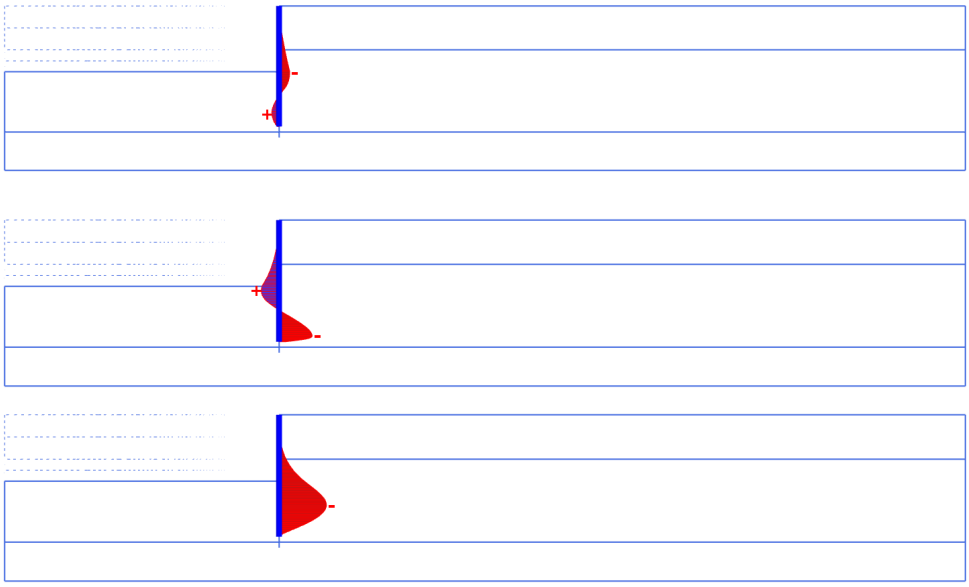

Figure 5.12. HS Forces in the sheet pile wall; axial force, max -39 kN/m , shear force, max -121 kN/m, bending moment, max -172 kNm/m, respectively.

5.5. Comparison

The two models generate similar results, the HS model behaves stiffer as expected. The HS model requires more input data than was available, and is thereby not treated right. Compared to the measured displacement both models show good results. It is not in the scope of this dissertation to evaluate the result more throughout, since the main purpose for this problem is to learn to work with the program and get a feel for a real object.

6. Plaxis 2D Example 2 - Piled raft foundation

6.1. Introduction

In this chapter a hypothetical piled raft foundation is analysed to illustrate the simplified analysis method described in Section 3.4.2. The piled raft modelled here is also present in Chapter 7, where it is analysed with Plaxis 3DFoundation.

6.2. Characteristics

The geometry of the piled raft is illustrated in Figure 6.1. The piled raft is situated on a single layer of soft clay and supports a uniform load of 30 kN/m^3. The piles are chosen to SP3 piles (Swedish standard), which are square pre-cast concrete piles with the width of 275 mm [5]. The raft and the piles where assumed to have a Young's modulus of 35 GPa. The firm rock is situated 40 m below the ground surface and the ground water table is situated three meters below the ground surface.

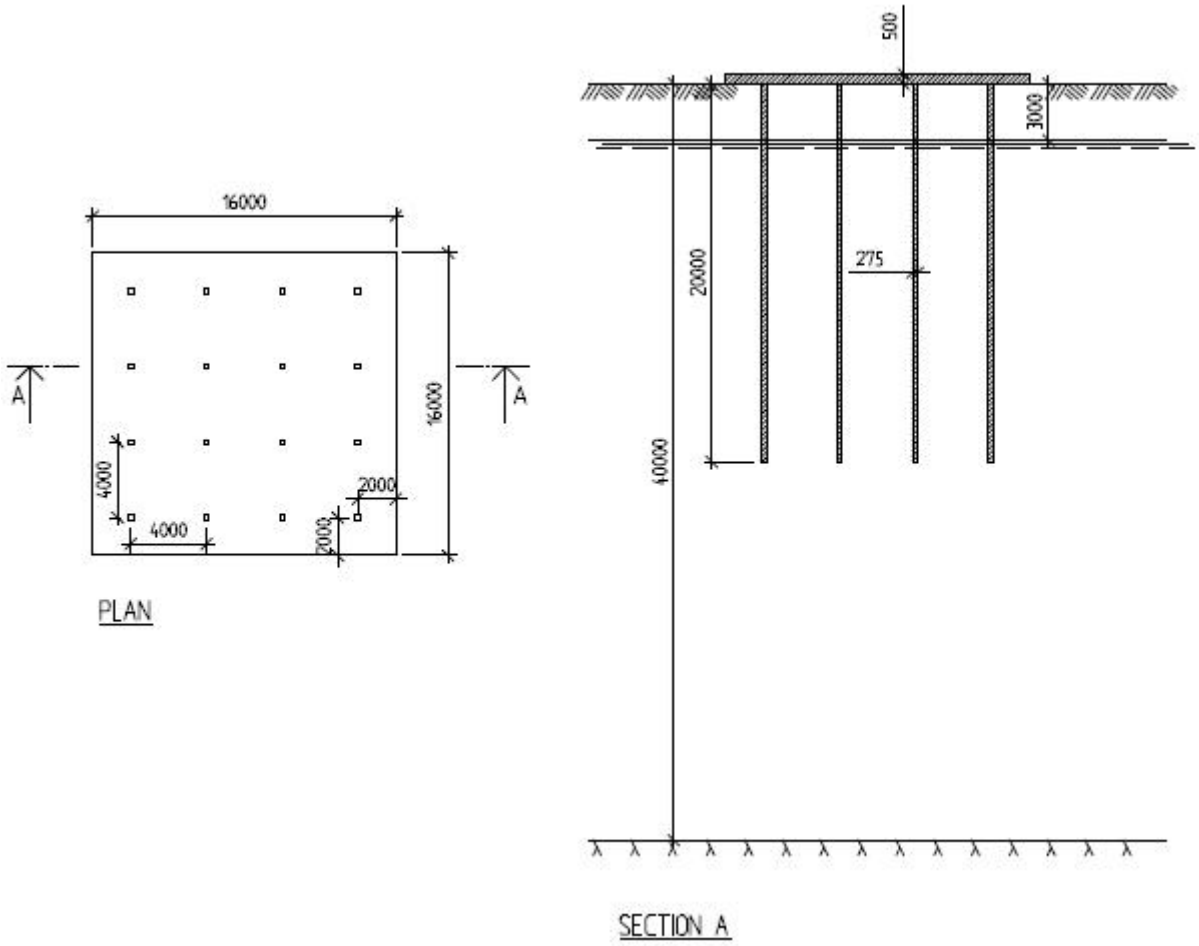

Figure 6.1. Configuration of the example [mm].

6.3. Model

6.3.1. Geometry

The geometry is presented in Figure 6.2.

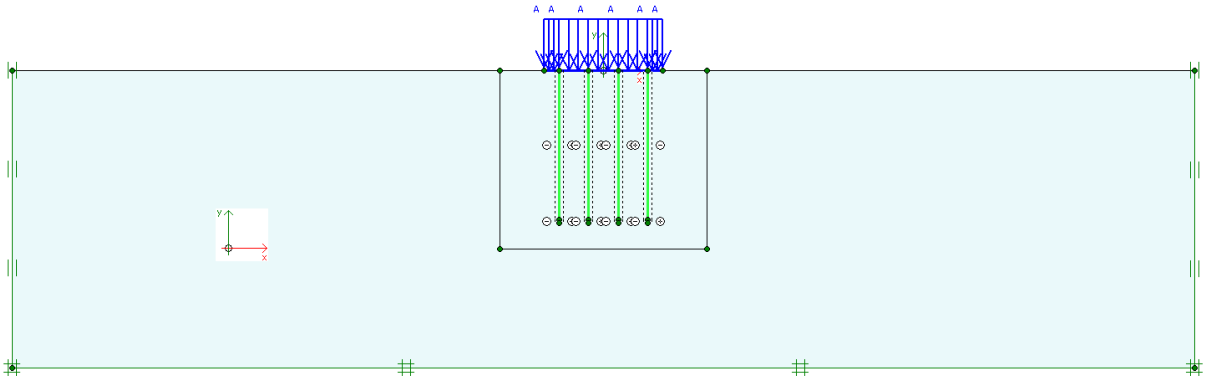

Figure 6.2. Geometry.

The model is 160x40 m^2. The displacements are prescribed to zero in both *x*- and *y*-direction in the bottom and in *x*-direction at the sides.

The cluster embracing the piled raft was introduced to prepare for a simple mesh optimisation, by using the "refine cluster" option during mesh generation.

Three different elements are present in the model; 15-node element for the clusters, plate element for the raft and the piles, and interface element for the interaction between the soil and the structural elements.

6.3.2. Material properties

The clay was modelled with the Mohr-Coulomb model with the input parameters presented in Table 6.1.

Table 6.1 Material parameters for the soil.

Input Parameter	Clay	Unit
Young's module, E'_{ref}	5000	kN/m^2
Poisson's ration, ν'	0.35	-
Saturated unit weight, γ_{sat}	18	kN/m^3
Unsaturated unit weight, γ_{unsat}	18	kN/m^3
Cohesion, c'_{ref}	4	kN/m^2
Friction angle, φ'	30	°
Dilatancy angle, ψ	0	°
Interface reduction factor, $R_{inter,eq}$	0.11	-

where the interface reduction factor was calculated using Eq. 3.19 and with the recommended value for R_{inter} in Chapter 4.2.1.

$$R_{inter,eq} = \frac{n_{p-row-i} A_s}{2L_r} R_{inter} = \frac{4 \cdot 0.275 \cdot 4}{2 \cdot 16} \cdot 0.8 = 0.11$$

The structural elements are modelled as plate elements and Plaxis requires four input parameters, i.e.: normal stiffness per meter depth, flexural rigidity per meter depth, Poisson's ratio and the weight per meter depth. The parameters used in this example are presented in Table 6.2.

Table 6.2 Material parameters for the structural elements.

Input Parameter	Raft	Pile	Unit
Normal stiffness, EA	$17.5 \cdot 10^6$	$662 \cdot 10^3$	kN/m
Flexural rigidity, EI	$365 \cdot 10^3$	4170	kNm^2/m
Poisson's ratio, v	0.2	0.2	-
Weigth, w	12.5	0.47	kN/m/m

Where the normal stiffness of the raft was calculated as

$$EA_{raft} = 35 \cdot 10^6 \cdot h_{raft} = 35 \cdot 10^6 \cdot 0.5 = 17.5 \cdot 10^6 \text{ kN/m}$$

and the bending stiffness of the raft

$$EI_{raft} = E \frac{b \cdot h^3}{12} = 35 \cdot 10^6 \frac{1 \cdot 0.5^3}{12} = 365 \cdot 10^3 \text{ kNm}^2\text{/m}$$

and the weight for the raft was calculated as

$$w = \gamma_{raft} \cdot h_{raft} = 25 \cdot 0.5 = 12.5 \text{ kN/m/m}$$

The normal stiffness for the plane strain piles was calculated using the "smeared" parameters from Eq. 3.15 , i.e.

$$EA_{psp} = EA_p \frac{n_{p-row-i}}{L_r} = 35 \cdot 10^6 \cdot 0.275^2 \frac{4}{16} = 662 \cdot 10^3 \text{ kN/m}$$

and the bending stiffness according to Eq. 3.16

$$EI_{psp} = EI_p \frac{n_{p-row-i}}{L_r} = 35 \cdot 10^6 \cdot \frac{0.275 \cdot 0.275^3}{12} \frac{4}{16} = 4170 \text{ kNm}^2\text{/m}$$

and the weight according to Eq. 3.17

$$w_{psp} = w_p \frac{n_{p-row-i}}{L_r} = 0.275^2 \cdot 25 \frac{4}{16} = 0.47 \text{ kN/m/m}$$

6.3.3. Mesh generation

The mesh was defined as fine dense and refined in the cluster surrounding the piled raft, since high stress gradients are expected there. The mesh is further refined at the end points of the plate element representing the raft. Interface elements are drawn beneath the piles to smoothen the mesh.

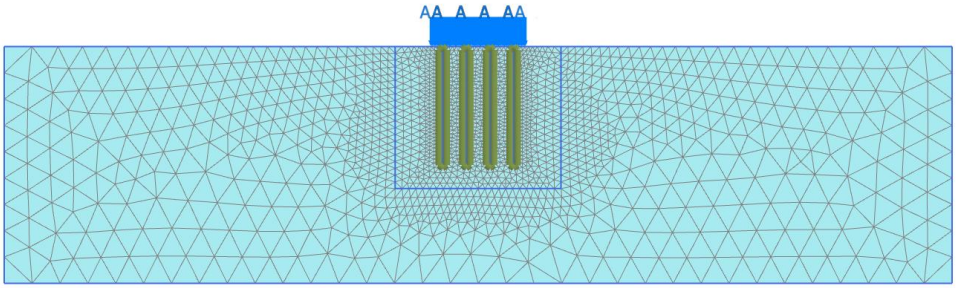

Figure 6.3. FEM-Mesh.

6.3.4. Initial condition

The initial stress-state was calculated with the K0-procedure and the initial water condition was calculated by the direct method, using the phreatic level. For this calculation no elements were activated.

6.3.5. Calculation

The calculation was performed as a plastic calculation and with standard settings for the iterative procedure. The long time settlements were studied and the undrained behaviour was thereby ignored. Just one calculation phase was defined, including activation of all the elements and the load.

6.4. Results

6.4.1. Deformation

The deformed mesh is illustrated in Figure 6.4 and the vertical displacement distribution is illustrated in Figure 6.5. The maximum settlement of the piled raft is 121 mm and the minimum is 105 mm, thus a differential settlement of 16 mm.

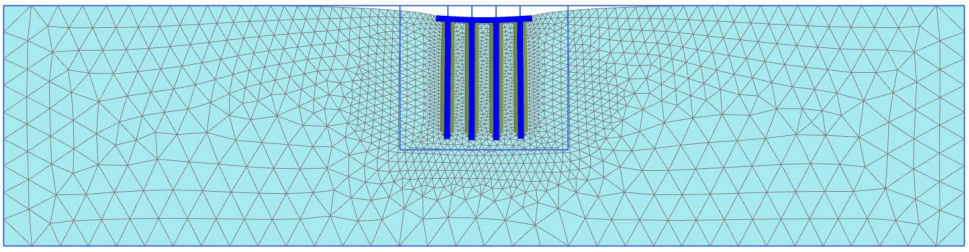

Figure 6.4. Deformed mesh.

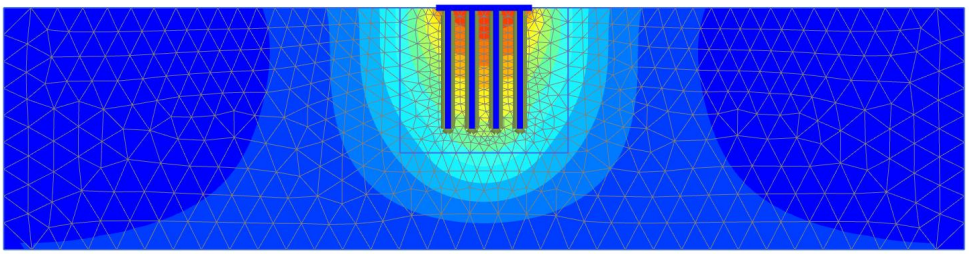

Figure 6.5. Distribution of the vertical displacement, max displacement -121 mm. Legend; red=-130 mm - blue=+10 mm.

6.4.2. Structural force

The distribution of bending moment in the raft is illustrated in Figure 6.6 and the maximum bending moment is 262 kNm/m.

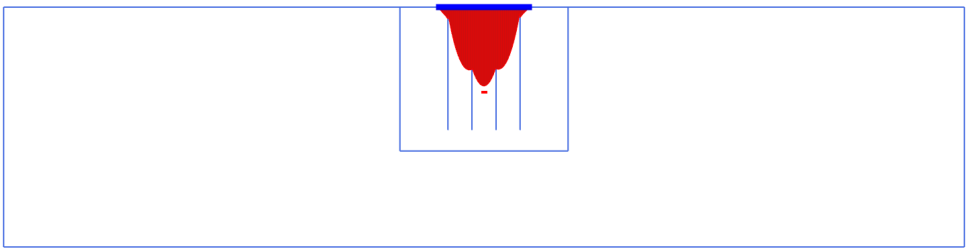

Figure 6.6. Distribution of bending moment.

The distribution of normal force for the plane strain piles is illustrated in Figure 6.7. The maximum normal forces in these piles are 98 kN and 77 kN, respectively, and are situated in the upper part of the pile as could be observed in the figure. Due to symmetry the other piles have the same normal force distribution.

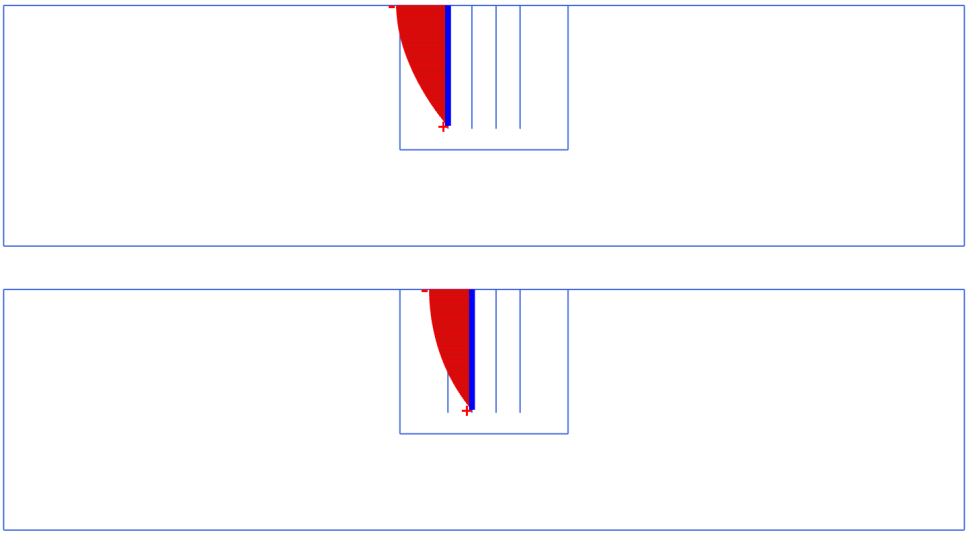

Figure 6.7. Distribution of normal force for two of the piles.

Summation of the four plane strain piles maximum normal forces, give us the total load taken by the piles. The total load could be divided with the total load to examine the load

distribution between pile and raft. This ratio is in this dissertation denoted ρ and is for this case

$$\rho = \frac{load\ carried\ by\ the\ piles}{total\ load} = \frac{N_1 + N_2 + N_3 + N_4}{(q + w_{raft})L_r + n_p w_{p,eq} L_p} = \frac{98 + 77 + 77 + 98}{(30 + 12.5)16 + 4 \cdot 0.47 \cdot 20} = 0.49$$

7. Plaxis 3DFoundation Example - Piled raft foundation

7.1. Introduction

In this chapter the hypothetical piled raft foundation analysed in Chapter 6 is analysed again using Plaxis 3DFoundation. This is carried out to get a better understanding for 3DFoundation and to present the general work process used in the parametric study in Chapter 8.

7.2. Characteristics

The same piled raft as in Chapter 6 is analysed and the characteristics is thereby presented in Chapter 6.2 and illustrated in Figure 6.1.

7.3. Model

7.3.1. Geometry

The model is160x160x40 m^3, thus the same width as the plane strain model. One work plane was defined at the ground level, shown in Figure 7.1. The work plane has two clusters, where the one in the middle was created to assign the raft and the load. A borehole was defined (the dot in the upper left corner in Figure 7.1), which is 40 meter deep and with the water level situated 3 meters below the ground surface. The bore hole was assigned the material properties (clay), as presented in Chapter 7.3.2.

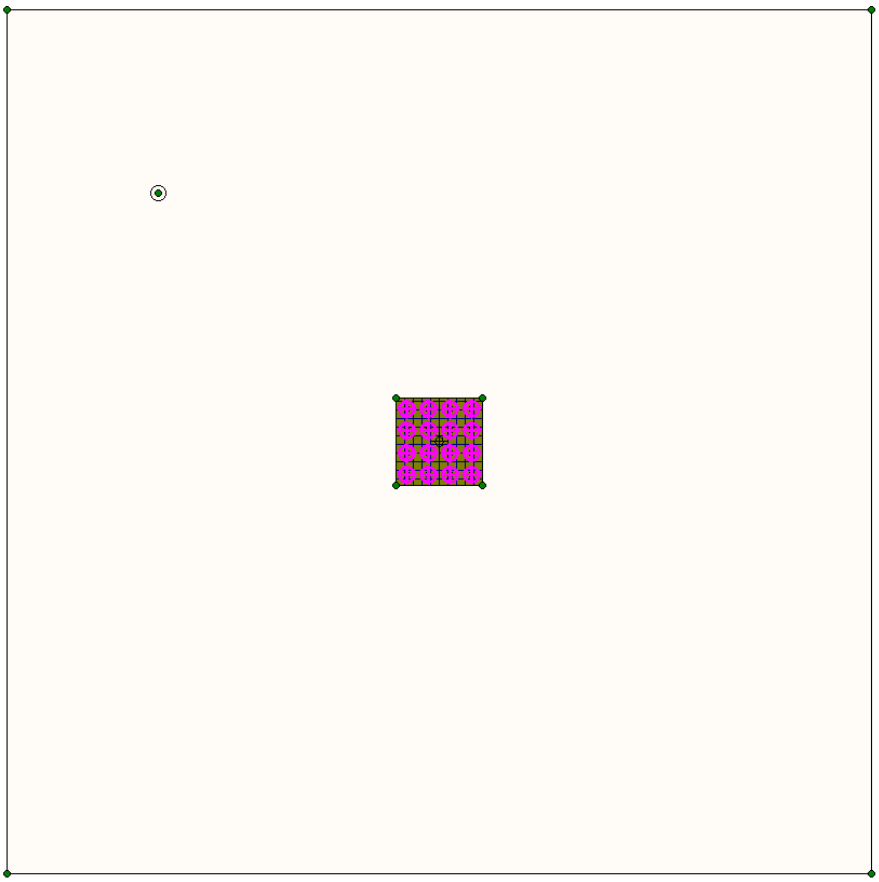

Figure 7.1. Geometry.

A three dimensional view of the model is illustrated in Figure 7.2, with the soil material turned off.

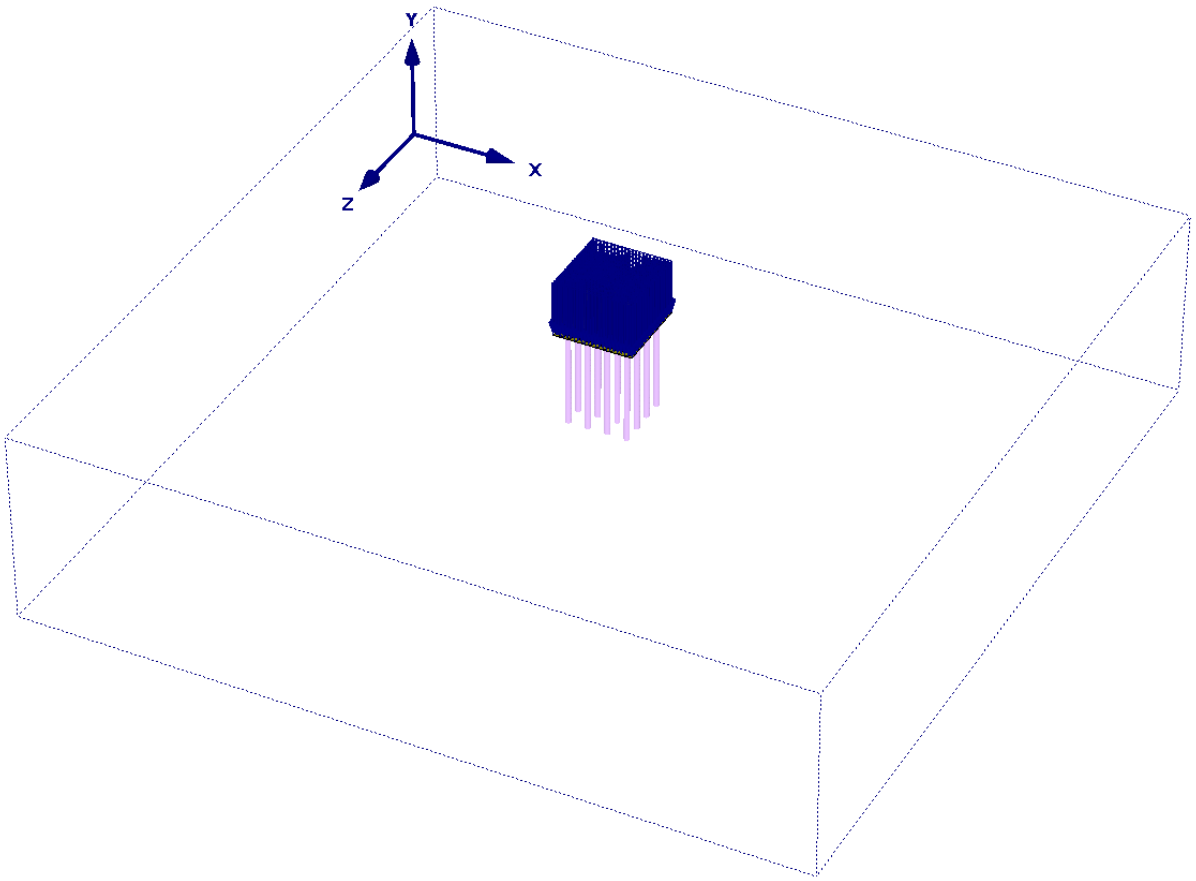

Figure 7.2. Geometry.

The boundary at the bottom of the model is totally rigid, and the side-boundaries are rigid in the two horizontal directions.

Three different elements are present in the model; volume element for the soil, floor element for the raft and embedded piles for the piles.

7.3.2. Material properties

The clay was modelled with the Mohr-Coulomb model with the input parameters presented in Table 7.1. The same input parameter as in Chapter 6 except R_{inter}, which is reset to the standard value of 0.8 (cohesive soil [12], Chapter 4.2.1).

Table 7.1. Material parameters for the soil.

Input Parameter	Clay	Unit
Young's module, E'_{ref}	5000	kN/m^2
Poisson's ration, ν'	0.35	-
Saturated unit weight, γ_{sat}	18	kN/m^3
Unsaturated unit weight, γ_{unsat}	18	kN/m^3
Cohesion, c'_{ref}	4	kN/m^2
Friction angle, φ'	30	°
Dilatancy angle, ψ	0	°
Interface reduction factor, R_{inter}	0.8	-

The raft was modelled as a floor, with isotropic stiffness and the input parameters as in Table 7.2. The piles were modelled as embedded piles with layer dependent shaft resistance and the input parameters as in Table 7.3.

Table 7.2. Material parameters for the floor.

Input Parameter	Floor	Unit
Young's modul, E	$35 \cdot 10^6$	kPa
Poisson's ration, ν	0.2	-
Unit weight, γ	25	kN/m^3
Height, d	0.5	m

Table 7.3. Material parameters for the embedded piles.

Input Parameter	Piles	Unit
Young's module, E	$35 \cdot 10^6$	kPa
Unit weight, γ	25	kN/m^3
Width, d	0.275	m

7.3.3. Mesh generation

A two dimensional mesh for the work planes was first conducted with medium dense net and the mesh was then refined four times in the cluster defining the raft. A three dimensional mesh was then created with fine dense. The final mesh is illustrated in Figure 7.3.

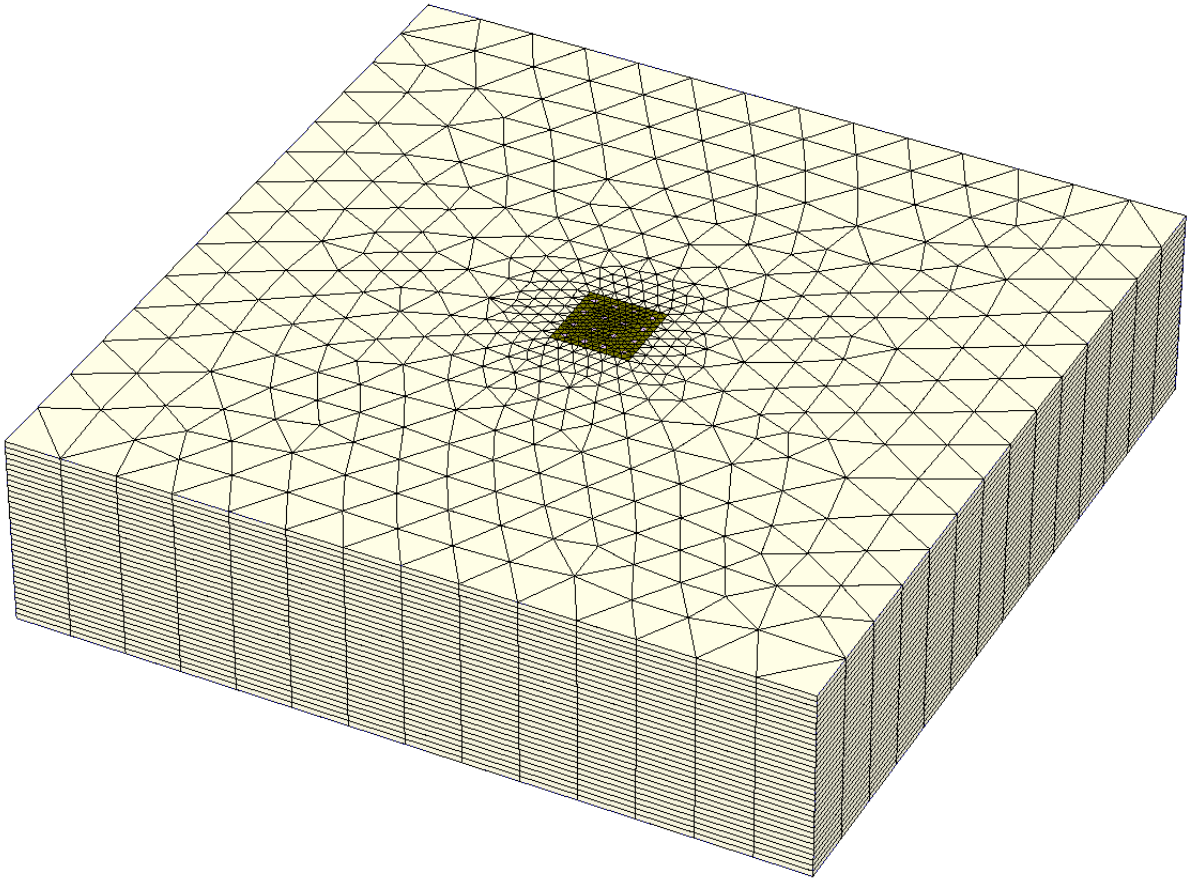

Figure 7.3. 3D Mesh.

7.3.4. Initial condition

The initial stress-state was calculated with the K0-procedure and the initial water condition was calculated by the direct method, using the phreatic level. For this calculation no elements were activated.

7.3.5. Calculation

The calculation was performed as a plastic calculation and with standard settings for the iterative procedure. The long time settlements were studied and the undrained behaviour was therefore ignored. Just one calculation phase was defined, including activation of all the elements and the load.

7.4. Results

7.4.1. Deformation

The deformed mesh is illustrated in Figure 7.4 and the distribution of vertical displacement is illustrated in Figure 7.5, for a section trough the piled raft. The maximum settlement of the piled raft is 56 mm and the minimum is 45 mm, thus a differential settlement of 11 mm.

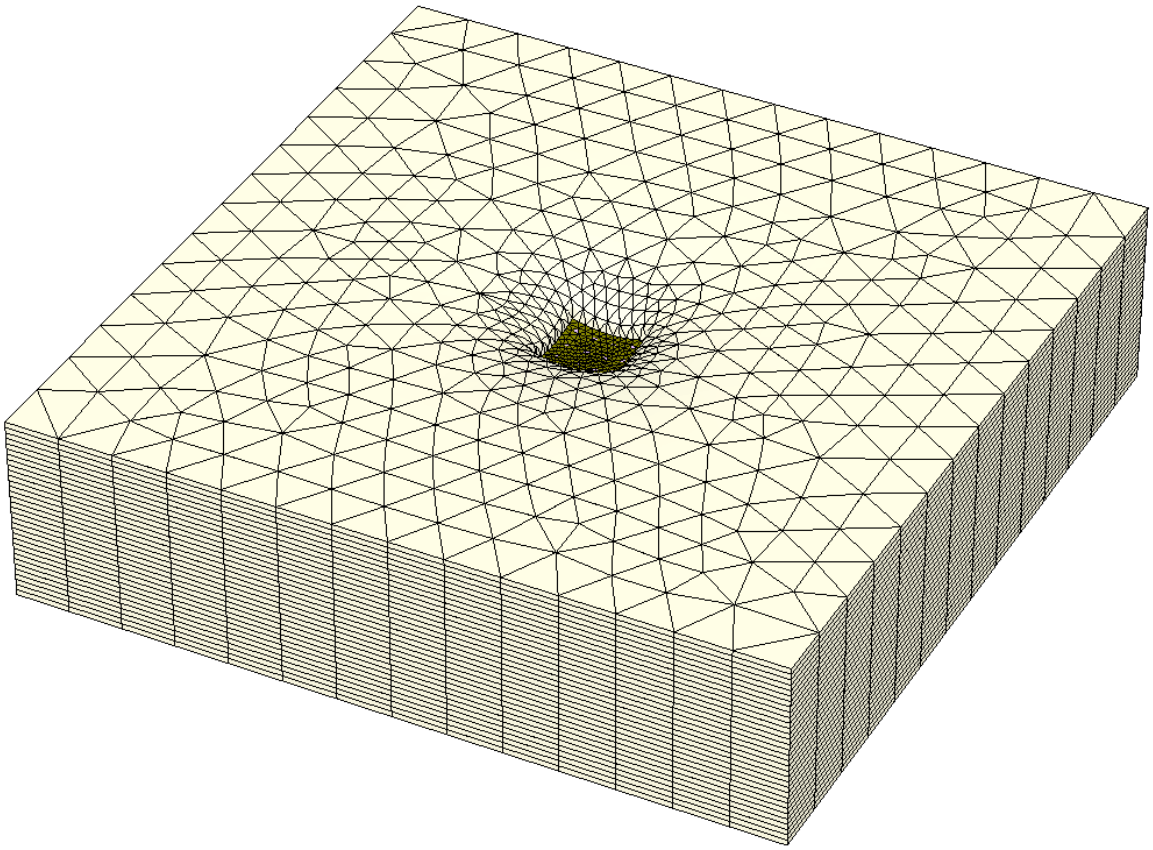

Figure 7.4. Deformed mesh.

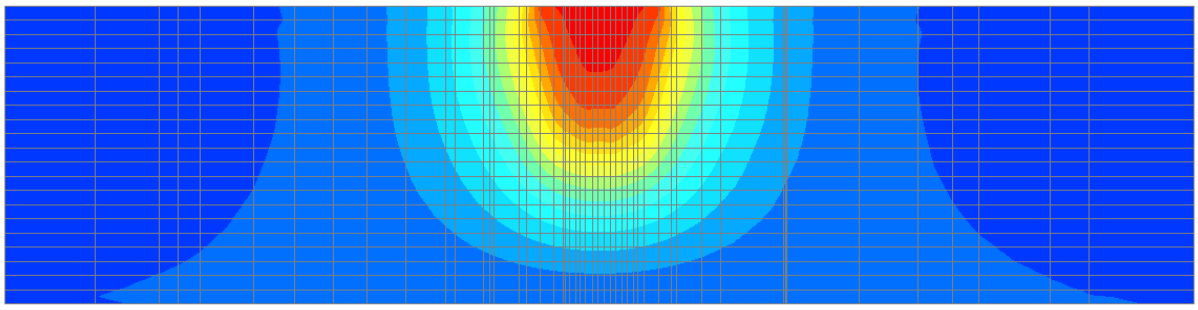

Figure 7.5. Vertical displacement distribution.
Legend; red=-56 mm – blue=+4 mm.

7.4.2. Structural force

The distributions of bending moment for the two main directions are illustrated in Figure 7.6. The first one is the bending moment in direction *x* for sections in *x*-direction, called M_{11}. The second one is the bending moment in direction *z* for sections in *z*-direction, called M_{22}. For

this case these two distributions are equal due to symmetry. The maximum bending moment is -129 kNm/m and the minimum is +31 kNm/m.

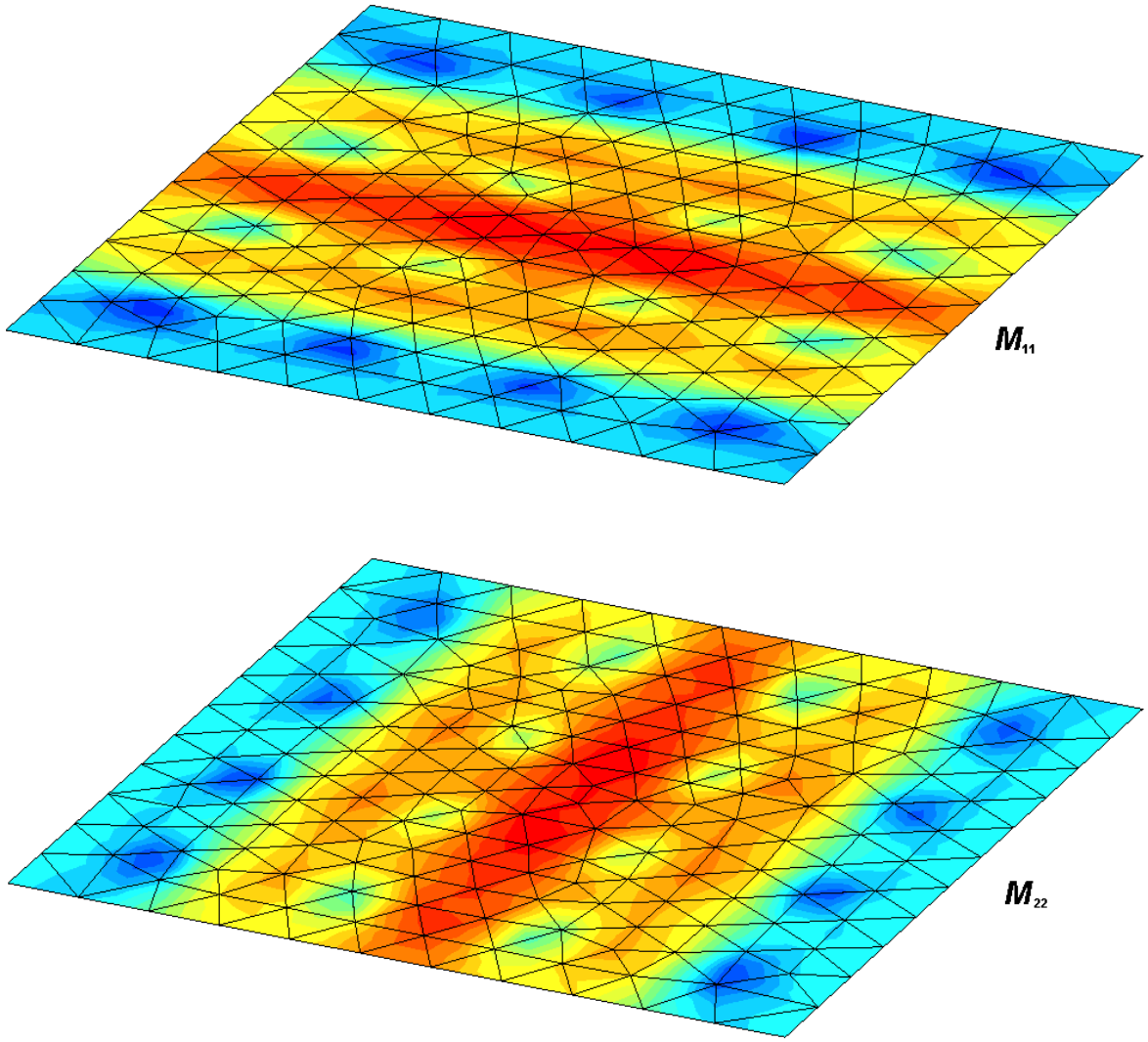

Figure 7.6. Distribution of bending moment, M_{11} and M_{22}.
Legend; red=-140 kNm/m – blue=+40 kNm/m.

The distribution of normal force for one of the piles is illustrated in Figure 7.7. The other piles have the same appearance with different magnitudes spanning between 414-500 kN.

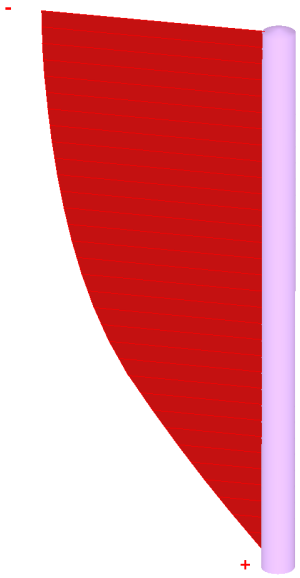

Figure 7.7. Distribution of normal force in a pile.

Summation of the sixteen piles maximum normal force, give us the total load taken by the piles. As for the plane strain piles in the 2D model the load carried by the piles is divided by the total load

$$\rho = \frac{load\ carried\ by\ the\ piles}{total\ load} = \frac{\sum_{i=1}^{16} N_i}{(q + w_{raft})L_r \cdot L_r + n_p \gamma_p A_p L_p} =$$

$$= \frac{(414 + 414 + 500 + 498) \cdot 4}{(30 + 12.5)16 \cdot 16 + 16 \cdot 25 \cdot 0.275^2 \cdot 20} = 0.64$$

where, symmetry has been used when calculating the load carried by the piles.

8. Parametric study - Piled raft foundations

8.1. Introduction

The purpose for this parametric study is to compare the plane strain model, explained in Chapter 3.4.2., with a full 3D analysis in Plaxis 3DFoundation, and examine the inaccuracies introduced in the plane strain model. The study has been limited to six piled rafts, three with varying pile spacing (Chapter 8.2) and three with varying raft shape (Chapter 8.3). Focus is thereby on two parameters, i.e. pile spacing and raft shape. The analyses of these six piled rafts are performed as the analysis in Chapter 6 and Chapter 7, and with the same characteristics (except pile spacing and raft shape). Subsequent to this study, two alternative methods are examined for the same piled rafts, one where the interface element is defined in a different manner (Chapter 8.4) and one where the shear strength reduction according to Eq. 3.18 is neglected (Chapter 8.5).

8.2. Pile spacing

8.2.1. Objects

The three piled rafts with varying pile spacing are illustrated in Figure 8.1, where piled raft B is the one calculated in Chapter 6 and 7.

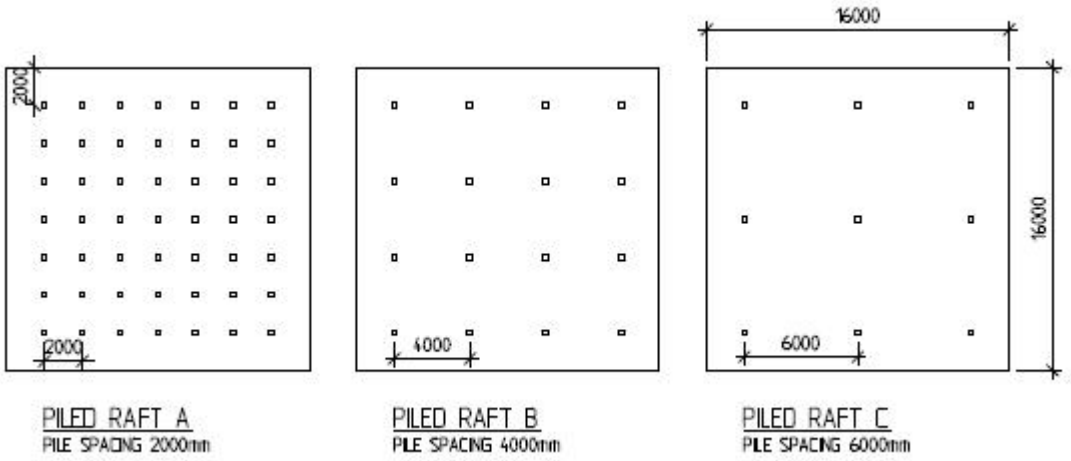

Figure 8.1 .The three piled rafts with varying pile spacing [mm].

8.2.2. Results

The results from the plane strain analysis in Plaxis 2D are presented in Table 8.1 and the results from the 3D analysis are presented in Table 8.2. As a comparison, the ratio between the results from the 2D analysis and the results from the 3D analysis (2D/3D) are presented in Table 8.3. All the results illustrated in the tables are maximum values.

Table 8.1. Response from the 2D analysis.

2D Response	PR A	PR B	PR C	Raft	Unit
Settlement	106	121	144	139	mm
Differential settlement	12	16	19	13	mm
Raft bending moment	206	262	270	200	kNm/m
Pile force, ρ	66	49	30	0	%

Table 8.2. Response from the 3D model.

3D Response	PR A	PR B	PR C	Raft	Unit
Settlement	52	56	67	91	mm
Differential settlement	9	11	18	25	mm
Raft bending moment	110	129	176	202	kNm/m
Pile force, ρ	77	64	48	0	%

Table 8.3. Comparison of the results from the two models.

2D/3D Response	PR A	PR B	PR C	Raft	Unit
Settlement	2.03	2.15	2.14	1.54	-
Differential settlement	1.31	1.45	1.02	0.54	-
Raft bending moment	1.87	2.03	1.53	0.99	-
Pile force, ρ	0.86	0.77	0.63	-	-

8.3. Shape of the piled rafts

8.3.1. Objects

The four piled rafts with varying raft shape are illustrated in Figure 8.2, where piled raft B1 is the same as piled raft B in the pile spacing study. Since the two dimensional models are calculated per meter, the same model applies for all piled rafts. The sections for the 2D models is taken in direction one and in the middle of the rafts. Calculations of sections in direction two are excluded in this work since the simplifications in a plane strain model are less correct in that direction.

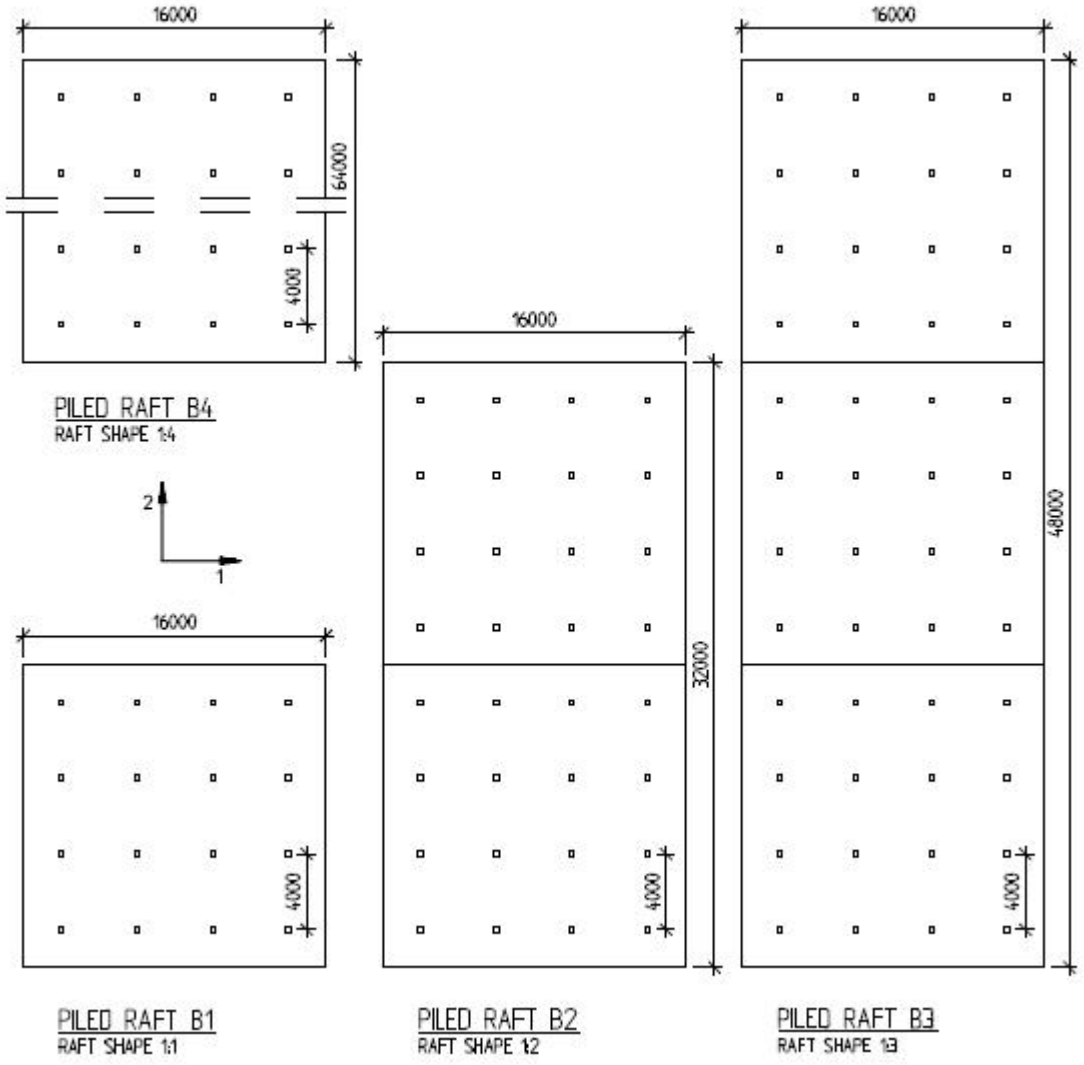

Figure 8.2 .The four piled rafts with varying raft shape [mm].

8.3.2. Results

The results from the 2D analysis are presented in Table 8.4 and the results from the 3D analysis are presented in Table 8.5. As a comparison, the ratio between the results from the 2D analysis and the results from the 3D analysis (i.e. 2D/3D) are presented in Table 8.6. All the results presented in the tables are maximum values. The bending moments presented in

the tables are M_{22}. This bending moment is the only one which can be compared since the 2D models can not calculate M_{11}.

Table 8.4. Results from analysis in 2D.

2D Response	B1-B4	Unit
Settlement	121	mm
Differential settlement	16	mm
Bending moment M_{22}	262	kNm/m
Pile force, ρ	49	%

Table 8.5. Results from the 3D analysis.

3D Response	PR B1	PR B2	PR B3	PR B4	Unit
Settlement	56	74	85	89	mm
Differential settlement	11	28	39	43	mm
Raft bending moment	127	124	125	125	kNm/m
Pile force, ρ	64	76	75	76	%

Table 8.6. 2D/3D-ratio.

2D / 3D Response	PR B1	PR B2	PR B3	PR B4	Unit
Settlement	2.15	1.63	1.43	1.36	-
Differential settlement	1.45	0.57	0.42	0.37	-
Raft bending moment	2.06	2.11	2.09	2.10	-
Pile force, ρ	0.77	0.64	0.65	0.64	-

The maximum bending moments in direction one for sections in the one-direction (M_{11} from the 3D models) are; 129 kNm/m, 110 kNm/m, 86 kNm/m and 78 kNm/m, respectively.

8.4. Alternative method 1 (AM1)

The above two sets of piled rafts are here calculated with an alternative method. In this method the interface material is defined in an alternative way. A new material is created (for the interface element) with the same properties as the surrounding soil, except for the strength properties which are reduced manually according to Eq. 4.1 and Eq. 4.2, with α_{ar} from Eq. 3.18 instead of using $R_{inter,eq}$. The interface reduction factor is reset to the standard value of 0.8 (cohesive soil [12], Section 4.2.1).

8.4.1. Pile spacing

The results from the 2D analysis are presented in Table 8.7 and the 2D/3D-ratios are presented in Table 8.8. The 3D results are the same as in Chapter 8.2.

Table 8.7. 2D response, using AM1.

2D Response AM1	PR A	PR B	PR C	Raft	Unit
Settlement	86	89	103	139	mm
Differential settlement	8	9	14	13	mm
Raft bending moment	151	163	220	200	kNm/m
Pile force, ρ	76	76	66	0	%

Table 8.8. 2D/3D-ratio.

2D / 3D AM1	PR A	PR B	PR C	Raft	Unit
Settlement	1.65	1.58	1.54	1.54	-
Differential settlement	0.88	0.80	0.75	0.54	-
Raft bending moment	1.38	1.26	1.25	0.99	-
Pile force, ρ	0.99	1.18	1.38	-	-

8.4.2. Shape of the piled rafts

The results from the 2D analysis are presented in Table 8.9 and the 2D/3D-rations are presented in Table 8.10. The 3D results are the same as in Chapter 8.3.

Table 8.9. Results from the analysis in 2D.

2D Response AM1	B1-B4	Unit
Settlement	89	mm
Differential settlement	9	mm
Bending moment M_{22}	163	kNm/m
Pile force, ρ	76	%

Table 8.10. 2D/3D-ratio.

2D / 3D AM1	PR B1	PR B2	PR B3	PR B4	Unit
Settlement	1.58	1.20	1.05	1.00	-
Differential settlement	0.80	0.31	0.23	0.20	-
Raft bending moment	1.28	1.31	1.30	1.31	-
Pile force, ρ	1.19	1.00	1.01	0.99	-

8.5. Alternative method 2 (AM2)

The piled rafts in Chapter 8.2 and 8.3 are also calculated with an alternative method where the interface reduction factor is reset to the standard value of 0.8 (cohesive soil [12], Chapter 4.2.1). The suggested reduction of shaft resistance in Section 3.4.2 is thereby neglected.

8.5.1. Pile spacing

The results from the 2D analysis are presented in Table 8.11 and the 2D/3D-ratios are presented in Table 8.12. The 3D results are the same as in Chapter 8.2.

Table 8.11. Results from analysis in 2D.

2D Response AM2	PR A	PR B	PR C	Raft	Unit
Settlement	87	82	86	139	mm
Differential settlement	8	8	11	13	mm
Raft bending moment	147	162	185	200	kNm/m
Pile force, ρ	76	80	78	0	%

Table 8.12. 2D/3D-ratio.

2D / 3D AM2	PR A	PR B	PR C	Raft	Unit
Settlement	1.66	1.46	1.28	1.54	-
Differential settlement	0.84	0.75	0.59	0.54	-
Raft bending moment	1.33	1.26	1.05	0.99	-
Pile force, ρ	0.99	1.25	1.63	-	-

8.5.2. Shape of the piled rafts

The results from the 2D analysis are presented in Table 8.13 and the 2D/3D-ratios are presented in Table 8.14. The 3D results are the same as in Chapter 8.3.

Table 8.13. Results from analysis in 2D.

2D Response AM2	B1-B4	Unit
Settlement	82	*mm*
Differential settlement	8	*mm*
Bending moment M_{22}	162	*kNm/m*
Pile force, ρ	80	*%*

Table 8.14. 2D/3D-ratio.

2D / 3D AM2	PR B1	PR B2	PR B3	PR B4	Unit
Settlement	1.46	1.11	0.97	0.93	-
Differential settlement	0.75	0.29	0.21	0.19	-
Raft bending moment	1.28	1.31	1.30	1.30	-
Pile force, ρ	1.25	1.05	1.07	1.05	-

8.6. Discussion

General

The two dimensional and the three dimensional models behave, in general, sound as the pile spacing and the shape of the piled rafts vary; decreasing settlements, differential settlements and bending moment as the number of piles increase, and increased load carried by the piles as number of piles increase, and converging results as the length of the raft is increased. The two dimensional models behave, in general, weaker than the three dimensional models, which was expected due to boundary effects.

Settlement

For the square piled rafts, the settlements were in general overestimated with the plane strain models, about 100-120% overestimation when using the original plane strain model and about 30% overestimation when using the alternative methods. A general overestimation was expected in the 2D models. However, the original plane strain model behaves remarkably weak and it seems like the interface becomes too weak when applying the reduction of shaft resistance with R_{inter}, probably because a low value of R_{inter} leads to too much slipping, according to Eq. 4.4.

While increasing the length of the piled raft the settlements in the 2D models move towards the one calculated in 3D, which is expected as the plane strain condition is more and more satisfactory. The alternative methods resemble the 3D model well for the piled raft shapes 1:2-1:4, with 2D/3D-ratios close to one. The settlements calculated with the AM1 converge towards the one calculated in 3D, while the AM2 models underestimates the settlement for PR B3 and PR B4 with 2D/3D ratios of 0.97 and 0.93, respectively.

Differential settlement

The differential settlements are in general underestimated in the 2D models, also for the model of the raft alone. This is a result of comparing the maximum differential settlements, without respect of the position of the settlements, which will differ in 2D and 3D. The maximum settlement is situated in the same point in 2D and 3D, i.e. in the middle of the piled raft. However, the minimum settlement in the 2D model is situated at the middle of the longer side, while the minimum settlement in the 3D model will be situated in the corners. This could be observed in Figure 7.4. However, this effect should diminish if the raft where stiffer.

As the length of the piled raft increases the effect of different positions of minimum settlement in 2D and 3D will increase. That is because the maximum differential settlement for the long rafts (PR B2- B4) will occur in direction two (Figure 8.2), while the plane strain models carried out is limited to calculate the differential settlement in direction one. Since the differential settlement is calculated in different direction one could argue that the 2D/3D-ratio for this result is irrelevant in Tab. 8.6, Tab. 8.10 and Tab. 8.14, but it illustrates a big disadvantage with the plane strain model, i.e. the differential settlement that can be calculated in a plane strain model is not in the critical direction. Assuming that the plane strain model is not used for sections in direction two, where the model would generate bad results, due to non plane strain conditions.

The 2D/3D-ratio for differential settlements calculated with the alternative methods seems to move towards one as the pile spacing decrease. This is expected since the wall elements used in the plane strain model more and more resemble the pile rows as the pile spacing decreases. This behaviour was also expected for the original plane strain model, but once again; the low R_{inter} seems to generate a too weak model. When comparing the alternative methods, one could see that the AM1 generates better results concerning differential settlement, especially for PR C, i.e. for piled rafts with large pile spacing.

Raft bending moment

The maximum bending moment in the rafts, were overestimated in all piled rafts analysed. All methods seem to coincide more closely with the three dimensional model as the pile spacing increase. The three methods seem to have a constant 2D/3D ratio as the raft length increases. The bending moment compared is M_{22}, which should be somewhat constant since the width of the piled raft is constant. For the original method the 2D/3D-ratio is about 2.1, and about 1.3 for the alternative methods. The bending moment M_{11} is equal to M_{22} for the square raft. However, for the non-square piled rafts M_{11} differs from M_{22}, but has not been calculated since no calculations for sections in direction two is performed, due to non plane strain conditions.

Pile force

The load taken by the piles is underestimated in the original plane strain models and overestimated in the alternative models. Generally, the two dimensional models describe the load carrying distribution with an over- and underestimation of about 0-40%. The piles are modelled too weak in the original plane strain models, which explain the underestimation of pile force. All methods seem to describe the distribution better as the pile spacing decreases. The AM1 describes the pile carrying very close to the three dimensional model and supersede the AM2, especially for PR B and PR C. For the long rafts the alternative models show a 2D/3D-ratio close to one; 0.99-1.01 using AM1 and 1.05-1.07 using AM2. The stiffer behaviour in the AM2 models were expected since the reduction of the shear strength is neglected.

9. Conclusion

The low value of R_{inter} that is introduced in the original plane strain model (Eq. 3.19), will generate too weak piled rafts and allow for the piles to slip too much. The errors are significant and it is recommended not to use this method.

By introducing a new material for the interface material as in AM 1, the slipping behaviour is avoided which leads to a better model. This model generates the best results in this study. However, the AM2 generates good results, especially when the pile spacing is small, and could be preferable since no modification of strength parameters is needed.

The inaccuracies occurring in the alternative plane strain models are more or less significant in all cases and the 2D models should be used carefully. Especially when calculating differential settlements or the bending moment in the longer direction. The plane strain models could generate similar results as a 3D model when pile spacing is narrow and the piled raft shape is greater than 1:2, i.e. when the problem is more two dimensional.

However, the piled rafts analysed are simple and as the problems get more complex the conclusions drawn here could be questionable, and the choice of model should lean towards a 3D model.

10. Further work

Simplifications and confinements have continuously been made, e.g. the piled rafts have been vertically and uniformly loaded, the soil cross section was very simple and had constant stiffness and strength parameters. Further work where different raft stiffness and load cases, are investigated would be interesting.

It would also, of course, be interesting to examine the methods used in this dissertation (or other methods for piled rafts) for real cases, where the results could be compared with measured data.

11. References

Printings

[1] Coduto C.P. (1999): *Geotechnical Engineering - Principles and Practices*, Prentice-Hall, United States of America

[2] Axelsson K. (2006): *Introduktion till GEOTEKNIK - jämte byggnadsgeologin, jordmaterialläran och jordmekaniken*, Inst. För Geovetenskaper, Uppsala Universitet

[3] Sällfors G. (2009): *Foundation Engineering VGT021 - Course Literature 2009*, Lunds Tekniska Högskola

[4] Eriksson P., Jendeby L., et. al. (2004): *Rapport 100 - Kohesionspålar*, Pålkommisionen, Linköping

[5] Olsson C. och Holm G. (1993): *Pålgrundläggning*, AB Svensk Byggtjänst och Statens Geotekniska Institut, Stockholm

[6] Tan Y.C. and Chow C.M (2004): *Design of piled raft foundation on soft ground*, GSM-IEM Forum: The roles of Engineering geology & geotechnical engineering in construction works, Department of Geology, University of Malaysia

[7] Poulos H.G. (2001): *Methods of Analysis of Piled Raft Foundation*, Technical Committee TC 18, ISSMGE

[8] Prakoso W.A. and Kulhawy F.H. (2001): *Contribution to Piled Raft Foundation Design*, Journal of Geotechnical and Geoenvironmental Engineering, vol. 127, No. 1, ASCE, 17-24

[9] Svensson H. och Staaf T. (2005): *Samverkansgrundläggning med kohesionspålar*, Exsamensarbete, Avd. Jord- och Bergmekanik, Kungliga Tekniska Högskola

[10] Brinkgreve R.B.J., Broere W., Waterman D. (2008): *PLAXIS 2D - Full Manual*, The Netherlands

[11] Brinkgreve R.B.J., Engin E., Swolfs W.M. (2010): *PLAXIS 3D - Full Manual*, The Netherlands

Oral contacts

[12] Johansson L. (2010-2011), Geotechnical engineer, Ramböll Sverige AB

Websites

[13] http://www.arcelormittal.com/sheetpiling/page/index/name/zsections (2010-11-10)